9-26-2019

Characterization of Corona Discharge for Ignition Improvement

Linyan Wang
University of Windsor

Characterization of Corona Discharge for Ignition Improvement

By

Linyan Wang

A Thesis
Submitted to the Faculty of Graduate Studies
through the Department of Mechanical, Automotive and Materials Engineering
in Partial Fulfillment of the Requirements for
the Degree of Master of Applied Science
at the University of Windsor

Windsor, Ontario, Canada

2019

Characterization of Corona Discharge for Ignition Improvement

by

Linyan Wang

APPROVED BY:

_____

X. Nie
Department of Mechanical, Automotive and Materials Engineering

_____

N. Eaves
Department of Mechanical, Automotive and Materials Engineering

_____

J. Tjong
Department of Mechanical, Automotive and Materials Engineering

_____

M. Zheng, Advisor
Department of Mechanical, Automotive and Materials Engineering

September 26, 2019

DECLARATION OF ORIGINALITY

I hereby certify that I am the sole author of this thesis and that no part of this thesis has been published or submitted for publication.

I certify that, to the best of my knowledge, my thesis does not infringe upon anyone's copyright nor violate any proprietary rights and that any ideas, techniques, quotations, or any other material from the work of other people included in my thesis, published or otherwise, are fully acknowledged in accordance with the standard referencing practices. Furthermore, to the extent that I have included copyrighted material that surpasses the bounds of fair dealing within the meaning of the Canada Copyright Act, I certify that I have obtained a written permission from the copyright owner(s) to include such material(s) in my thesis and have included copies of such copyright clearances to my appendix.

I declare that this is a true copy of my thesis, including any final revisions, as approved by my thesis committee and the Graduate Studies office, and that this thesis has not been submitted for a higher degree to any other University or Institution.

ABSTRACT

Advanced spark ignition (SI) engines may better operate under lean or diluted conditions for fuel efficiency improvement. Under lean or diluted conditions, the ignition and complete combustion of the mixture is a challenge with conventional spark plugs. The small spark gap with limited spark energy delivery and the associated heat loss to the ground electrode, remain to be an unsolved problem. This research explores the corona discharge as an alternative ignition technology to counter the challenges of lean or diluted combustion, including the intensive gas flow condition. Without an adjacent ground electrode, the corona discharge tends to generate a larger ignition volume and multiple flame kernels. The study is based on an in-house designed alternating-current (AC) corona system with adjustable electrical parameters. By controlling stable corona discharge, the plasma length is characterized, including the effects of discharge voltage, discharge duration, discharge frequency, and background conditions on corona discharge. Subsequently, ignition research is conducted to combustible mixtures, in constant volume chambers, to demonstrate the ignition capability of corona discharge under both quiescent and forced flow conditions. The preliminary test results of plasma-enhanced combustion are discussed to help future studies on clean combustion innovations.

DEDICATION

This work is dedicated to my parents.

ACKNOWLEDGEMENT

I would like to express my sincere gratitude to my supervisor, Dr. Ming Zheng, who gave me the precious opportunity to join the research group. His patient guidance and strong support are continuous encouragement on my work currently and in the future.

I appreciate the invaluable assistance and feedback from my committee members – Dr. Jimi Tjong, Dr. Xueyuan Nie, and Dr. Nickolas Eaves.

I wish to extend my acknowledgement to everyone in the Clean Combustion Engine lab. I would like to thank all my colleagues – Dr. Meiping Wang, Dr. Shui Yu, Dr. Xiao Yu, Dr. Qingyuan Tan, Dr. Shouvik Dev, Dr. Kelvin Xie, Zhenyi Yang, Hua Zhu, Navjot Sandhu, Divyanshu Purohit, Simon Leblanc and Li Liang for their support in my research.

The work presented in this manuscript is based on the contributions of many current and former research associates. I would like to thank Dr. Shui Yu, Dr. Kelvin Xie and Dr. Qingyuan Tan for their previous work on the setup of the corona ignition system. I sincerely thank Dr. Xiao Yu, who gave me valuable assistance and suggestions on this research. I am also very grateful to Shuai Huang from Shanghai Jiao Tong University, for many enlightening discussions and future plans during the course of this research.

Finally, I would like to thank my parents for their love and support all the time.

TABLE OF CONTENTS

DECLARATION OF ORIGINALITY III

ABSTRACT IV

DEDICATION V

ACKNOWLEDGEMENT VI

LIST OF FIGURES IX

LIST OF ABBREVIATIONS/SYMBOLS X

CHAPTER 1 INTRODUCTION 1

1.1 Spark Ignition Systems 1

1.2 Alternative Ignition Systems for SI Engines 4

1.3 Corona Discharge 5

1.3.1 Physical Principles of Corona Discharge 5

1.3.2 Applications of Corona Discharge 6

1.3.3 Existing Corona Ignition Systems 7

1.3.4 Main Benefits and Challenges of Corona Ignition Systems 8

1.3.5 Plasma-assisted Combustion and Applications 10

1.4 Thesis Outline 10

CHAPTER 2 EXPERIMENTAL SETUPS 12

2.1 High-frequency Ignition Driver 12

2.2 Experimental Setup with a CVCC 14

2.3 Data Acquisition 16

2.3.1 Optical Data Acquisition 16

2.3.2 Numerical Data Acquisition 17

CHAPTER 3 CHARACTERIZATION OF CORONA PLASMA LENGTH 19

3.1 Effect of Discharge Voltage 19

3.2 Effect of Discharge Duration 22

3.3 Effect of Discharge Frequency 23

3.4 Effect of Background Media and Pressure 25

CHAPTER 4 IGNITION CAPABILITY OF CORONA DISCHARGE 28

4.1 Effect of Discharge Voltage 28

4.2 Ignition Capability of Corona Discharge under Quiescent Conditions 30

4.3 Ignition Capability of Corona Discharge under Forced Flow Conditions 31

4.4 Flame Propagation Enhancement by Corona Discharge 32

CHAPTER 5 CONCLUSIONS AND FUTURE WORK 36

5.1 Conclusions 36

5.2 Future Work 37

REFERENCES/BIBLIOGRAPHY 39

APPENDICES 46

Appendix A 46

Appendix B 47

LIST OF PUBLICATIONS 51

VITA AUCTORIS 53

LIST OF FIGURES

Figure 1- 1. TCI system with secondary current and gap voltage waveforms for a typical spark event. 2
Figure 1- 2. Ignition technologies with different working frequency ranges. 3
Figure 1- 3. Ignition technologies with different working frequency ranges. 4
Figure 1- 4. Corona discharge. 6
Figure 1- 5. Main advantages of corona discharge. 9
Figure 2- 1. A high-frequency ignition driver circuit of the corona ignition system. 13
Figure 2- 2. Schematic of corona ignition system with shadowgraph imaging. 15
Figure 2- 3. The command signal, measured secondary voltage signal, and measured current signal during corona discharge. 18
Figure 3- 1. The discharge voltage waveforms of corona vs. spark under atmospheric condition. 19
Figure 3- 2. The peak discharge voltages of corona vs. the breakdown voltages of conventional spark under different pressures. 21
Figure 3- 3. The effect of discharge voltage on corona plasma length. 22
Figure 3- 4. Pressure and duration effect on corona plasma length. 23
Figure 3- 5. The corona plasma length within the selected frequency range of the command signals. 24
Figure 3- 6. The maximum length of the discharged streamers within the selected operating range of frequency. 24
Figure 3- 7. Direct images of corona discharge using different background gases and under different pressures. 26
Figure 3- 8. The equivalent capacitance with corona discharge under different pressures. 27
Figure 4- 1. Shadowgraph images of corona ignition in the propane-air mixture. 29
Figure 4- 2. Areas of the flame fronts under different discharge voltage levels. 30
Figure 4- 3. Shadowgraph images of spark and corona ignition under quiescent condition. 31
Figure 4- 4. Shadowgraph images of the spark and corona ignition cases under quiescent and forced flow conditions. 32
Figure 4- 5. Discharge currents of 1 ms corona ignition, one post and four post pulses corona-assisted ignition. 33
Figure 4- 6. Shadowgraph images of corona ignition and corona assisted flame propagation. 34
Figure 4- 7. Flame areas of corona ignition and corona assisted flame propagation. 35

LIST OF ABBREVIATIONS/SYMBOLS

Abbreviations

AC	Alternating Current
ACIS	Advanced Corona Ignition System
BDI	Barrier Discharge Ignition
CVCC	Constant Volume Combustion Chamber
DC	Direct Current
EGR	Exhaust Gas Recirculation
HF	High Frequency
NPD	Nanosecond Pulsed Discharge
PCBs	Printed Circuit Boards
RF	Radio Frequency
SI	Spark Ignition
TCI	Transistor Coil Ignition
TTL	Transistor-transistor Logic

Symbols

C	Capacitance	(F)
f	Frequency	(Hz)
f_r	Resonant frequency	(Hz)
I	Root-Mean-Square values of discharge current	(A)
I_s	Discharge current of corona	(A)
L	Inductance	(H)
P	Instantaneous power of corona discharge	(W)
R	Resistance	(Ω)

V	Root-Mean-Square values of discharge voltage	(V)
V_c	Discharge voltage of corona	(V)
$\|Z\|$	Magnitude of the impedance	
$\emptyset$	Phase difference between voltage and current	
θ	Phase difference between the discharge voltage and current	

CHAPTER 1 INTRODUCTION

Automotive engines are facing increasingly stringent fuel efficiency and exhaust emissions regulations[1]. Recent spark ignition engine research indicates that the lean/diluted combustion can help in attaining high fuel efficiency targets[2,3]. However, under lean/diluted conditions, the ignition and subsequent flame propagation with a conventional spark plug tend to be unreliable[4-6]. Numerous ignition improvements have been attempted in the recent past to enhance the lean/diluted combustion processes[7,8,9].

1.1 Spark Ignition Systems

A simplified circuit of a conventional transistor coil ignition (TCI) system is shown in Figure 1-1. The TCI system consists of a transistor, a pair of ignition coils, and a spark plug. The transistor acts as a switching device, while the pair of ignition coils acts as a high voltage transformer[10]. Prior to initializing an ignition event, the transistor is switched on so that the current starts to flow through the primary coil of the transformer, storing energy in its electric field. In Figure 1-1, the current and voltage waveforms are presented for a typical spark event, in which the charging duration of the primary coil is 3 ms. During the charging duration, the current in the primary coil increases gradually. When the primary coil's electric field is cut off, the stored magnetic energy is released in three phases[11]. First, a high voltage is generated to the spark plug resulting in an electric field across the spark gap. This electric field accelerates the electrons and ions between the gap which eventually generates a conductive plasma channel connecting the gap. This stage is called the breakdown phase. The required breakdown voltage depends on the media pressure, temperature, composition, and the gap size and shape[10]. The spark gap is defined as the space between the ground electrode and the central electrode of a spark

plug. The breakdown phase is followed by the arc phase during which the energy stored in the coil, and the structure capacitance starts to release. Finally, the discharge process transits into the glow phase, releasing most of the stored electrical energy. The remaining energy from the secondary coil is dissipated in the plasma by means of a pattern of depleting current through the spark channel.

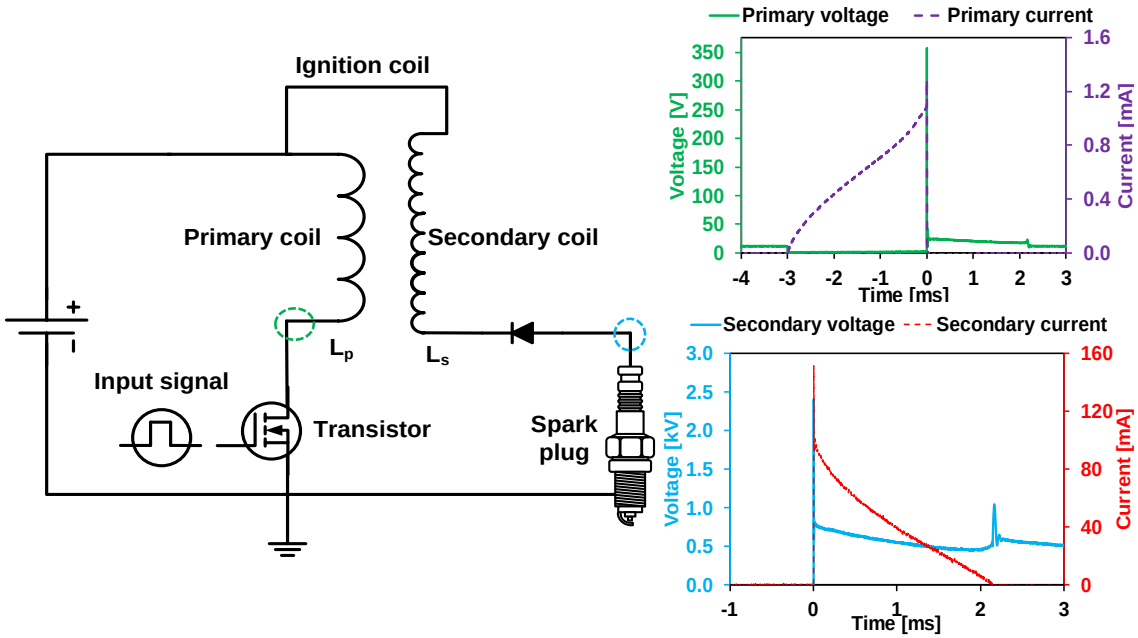

Figure 1- 1. TCI system with secondary current and gap voltage waveforms for a typical spark event.

Three cycles of a cylinder pressure curve of an SI engine is shown under the timeline in Figure 1-2. The yellow and green waveforms represent the fuel injection signal and spark signal, respectively. The fuel injection command and timing are at the same time point, while the spark timing delays the spark command with the charging duration. Thus, the response time of the conventional spark ignition system is depending on the charging duration of the ignition coil.

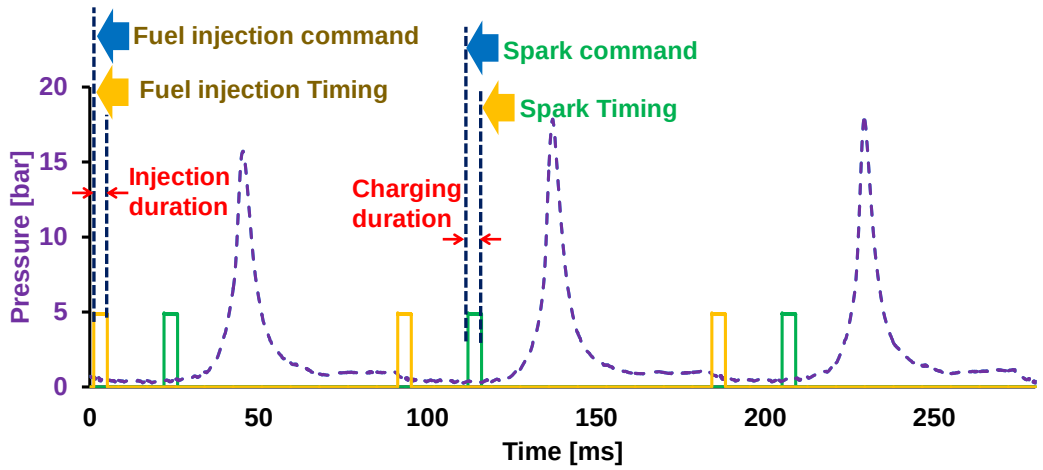

Figure 1- 2. Ignition technologies with different working frequency ranges.

According to the previous research, the lean/diluted combustion in SI engines may increase cycle-to-cycle variations[12,13]. One of the drawbacks of the conventional spark ignition system is the limited deployable size of a spark gap. The spark gap commonly is in a range of 0.4~1.5 mm. In order to succeed in the breakdown, high cylinder pressure engines tend to use small gap size. In addition, the ground electrode may quench the initial flame kernel because of the heat loss.

Even under limited gap size, the length of the spark plasma can still be increased by the application of cross-flow to the spark gap. Studies have shown that, in the flow field, the plasma channel during the glow phase tends to deflect or stretch out of the spark gap along the flow direction[14]. Therefore, while this extended spark length can provide additional surface area for the flame kernel to develop, the energy density along the spark channel is reduced largely in proportion to the flow velocity. Consequently, the local energy might not be sufficient to generate a self-sustaining flame kernel. The increasing of the discharge current makes it possible to maintain the spark channel and thus to suppress the need for restrike[15]. However, higher energy TCI systems may accelerate the

thermal-electric wear of the spark electrodes, and even risk overheating the transformer. In some cases, an increase in the spark gap size may help to succeed in the ignition[15]. However, a larger gap size requires a higher breakdown voltage. The maximum breakdown voltage is ultimately limited by the design parameters of ignition coils and dielectric capability of the spark plug ceramic[10].

1.2 Alternative Ignition Systems for SI Engines

In recent years, the ignition techniques in SI engines are advancing in an accelerated manner. The main objectives of a significant number of ignition research are to increase the delivered ignition power or energy, enlarge the ignition site volume, deploy multiple ignition sites, and actively control the energy delivery in real time[16]. Some of the ignition technologies with respect to their working frequency ranges are shown in Figure 1-3[17,18]. The discharge duration of a conventional TCI system is approximately 1~5 ms, including the breakdown, arc, and glow phases. The frequency of discharging events with the TCI system can reach 200~1000 Hz. The dual-coil offset/ignition system usually works under 1~20 kHz, being able to prolong the glow phase with thermal plasma[19].

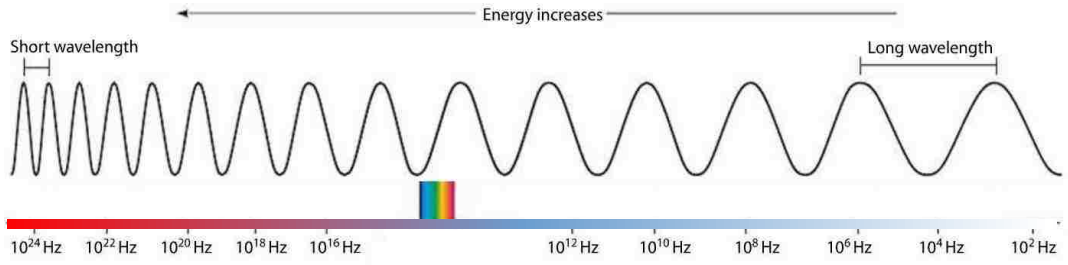

	Laser	Microwave	Nanosecond Discharge	RF Corona	Dual-coil	TCI
Frequency	500~1000 THz	2.4~30 GHz	20~100 MHz	0.1~3 MHz	1~20 kHz	200~1k Hz
Ignition method	Laser Induced Breakdown	Electromagnetic Field / Breakdown	Cold Plasma	Cold Plasma	Thermal Plasma	Thermal Plasma

Figure 1- 3. Ignition technologies with different working frequency ranges.

Several alternative ignition technologies are being explored in modern ignition research[4]. The radio-frequency (RF) based systems contain a corona ignition system and a barrier discharge ignition (BDI) system[20,21]. Other technologies include microwave ignition system[22,23]and laser ignition[24]. The majority of these systems are designed for lean/diluted combustion applications.

1.3 Corona Discharge

The corona discharge has shown a promising ability to promote ignition owing to its high discharge energy and large ignition volume[25]. Instead of forming a small thermal plasma channel as is in the conventional TCI system, corona discharge produces larger and less-constrained plasma channels with multiple ignition sites. The corona discharge concept presented in this thesis is an RF plasma discharge. A resonant principle is applied to produce alternating current (AC) corona plasma. In the present research, the frequency range of the AC is approximately 800 kHz to 3 MHz. It is expected to generate a larger ignition volume compared with the spark ignition system. It may result in a larger initial flame kernel, which may aid in the ignition of lean/diluted mixtures[26].

1.3.1 Physical Principles of Corona Discharge

The geometric design of a corona ignitor differs from a traditional spark plug. There is no ground electrode of a corona ignitor, and the tip of the central electrode should be an antenna, often sharped as a needle for energy discharge. A typical corona discharging event is shown in Figure 1-4. The waveforms show the high-frequency command signal, secondary voltage, and secondary current.

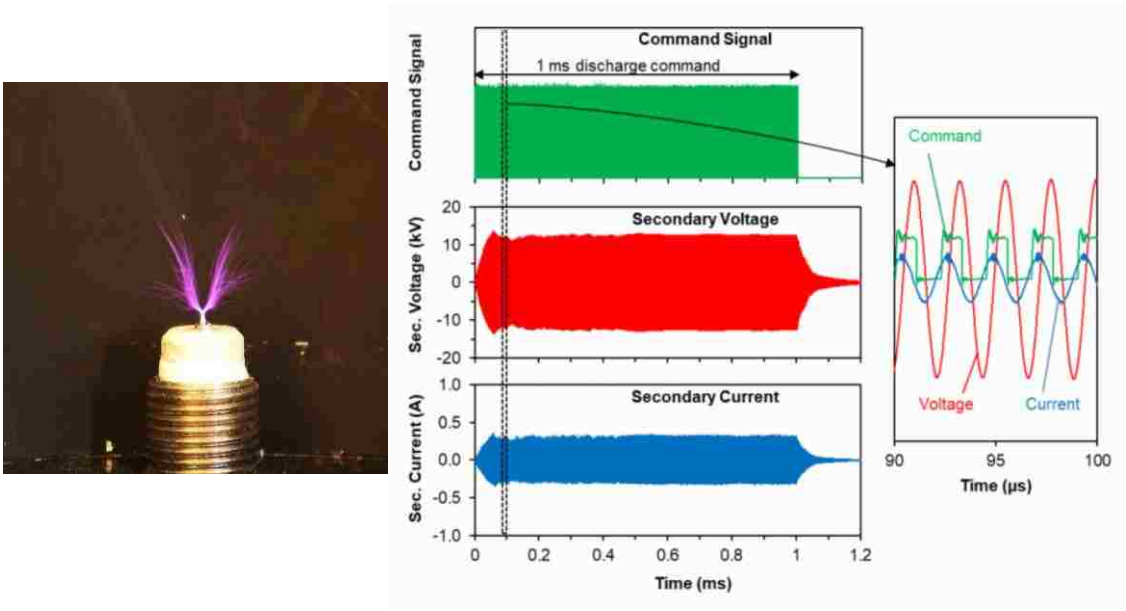

Figure 1- 4. Corona discharge.

When a high voltage is applied to the electrode, the electrons in the electrode are accelerated to high speed. Consequently, the gas molecules around the ignitor tip are ionized. This ionization process causes an avalanche effect leading to the breakout of the gas media[27,28]. During the corona discharge processes, the ionized region grows quickly, forming separate filaments, which look similar to the roots of a tree. These are called the streamers of corona discharge and are the potential ignition sites, which produce a larger ignition volume.

1.3.2 Applications of Corona Discharge

There are many practical applications of corona discharge in industry, including the automotive, semiconductor, environmental, medical industry, etc[29-31].

The first commercial implementation of the corona discharge phenomenon was the electrostatic precipitator in 1905[32]. A mechanical rectifier and an AC transformer for high-voltage supply were applied. More recently, corona surface treatment technologies

are used for surface modifications on plastics, semiconductors, glass, metals, and ceramics. Furthermore, the extreme difference in density and electrical conductivity of metallic and nonmetallic materials provides an excellent condition for the application of corona electrostatic separation in printed circuit boards (PCBs) recycling[33]. Additionally, the treating of wool fabric with low-temperature plasmas in O_2, Ar, N_2, and CF_4 gases improves the laundry shrink resistance in spite of considerably increased frictional coefficients[34].

In some environmental applications, a key feature of the plasma process is that it generates a large flux of energetic electrons, which can be used to initiate or enhance a variety of chemical, biological, and physical reactions[35]. In the 1980s, corona technologies started making numerous progress in removing gaseous pollutants, mostly NO_x and SO_x[36,37].

The technique of RF corona ignition has raised a lot of attention in recent years and moved to the forefront of ignition research[38,39]. Other interesting practical applications of corona discharge are the corona ignition analysis and the plasma-assisted combustion[40,41].

1.3.3 Existing Corona Ignition Systems

Although the large-scale applications of corona ignition systems in vehicle production have not been reported, vigorous developments of the RF corona ignition technologies have been undertaken by a number of automotive technology companies. Notable developments are the Advanced Corona Ignition System (ACIS) from Federal-Mogul and the Eco-flash System from BorgWarner[42,43]. According to the reported results, ACIS has

shown better performance compared with the conventional spark ignition. It produces a larger initial ignition volume, faster mass-burn fraction, and reduced cycle-to-cycle variations[44].

GM Global Research and Development has examed the performance of ACIS in both optical engines and turbocharged, direct-injected, multi-cylinder engines[45]. The system is tested in the optical engines with different combustion strategies to evaluate its capabilities and limitations. For a stoichiometric mixture with the same spark advance timing, the ACIS has shorter ignition delay and faster flame kernel formation compared with the spark plug system. In the tests, the ACIS also performs better than the spark plug system under the condition of 20% exhaust gas recirculation (EGR). However, the ACIS requires higher ignition voltage to avoid misfires, mainly due to the increasing pressure at the time of ignition.

1.3.4 Main Benefits and Challenges of Corona Ignition Systems

The main advantages of RF corona ignition are the large ignition volume, flexible combustion control, and continuous energy delivery, as shown in Figure 1-5. Without the limitation of spark gap size, the corona release may result in larger ignition volume and multi-spot flame kernels[46,47]. Without the heat loss on the ground electrode, the RF energy can be efficiently delivered to the combustible gas. According to the results, it is often believed that corona discharge may promote the initial flame propagation, extend the flammability limits, and improve flame stability[39-48].

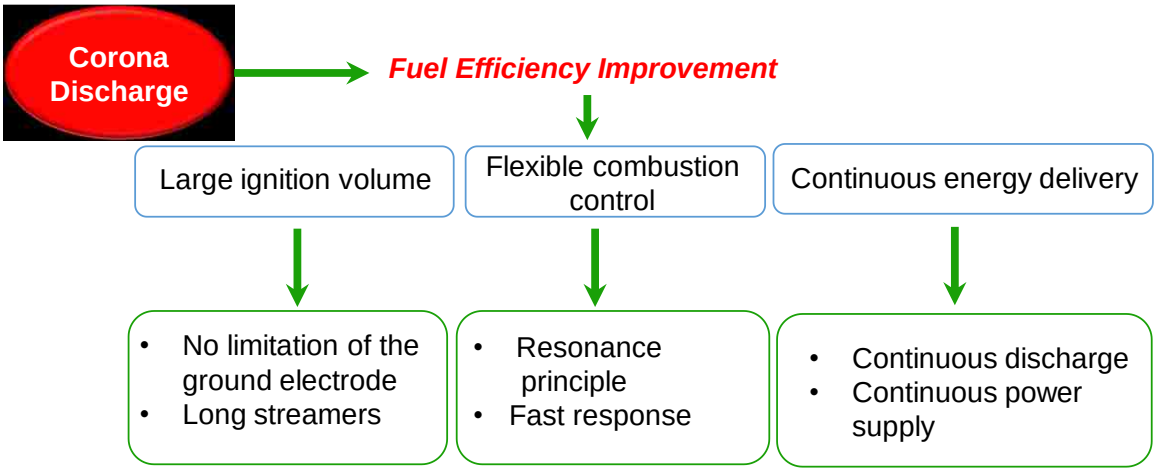

Figure 1- 5. Main advantages of corona discharge.

One of the major challenges of RF corona ignition is the avoidance of arcing. When a metal surface comes close to the streamers, an arc tends to form. The arc may happen with a sudden surge in both discharge voltage and current. Consequently, this would lead to an outage in the discharge voltage and current owing to the limited power supply. In a corona system, the duration and intensity of an arc may not be sufficient to provide reliable ignition. The arcing may also result in excessive wear of the igniter tip. Thus, chamber geometry is important. The corona arcing is especially problematic in downsized engines.

Additionally, the distribution of the electric field close to the igniter tip can be easily distorted by external disturbances[48-51]. The lab test results by Federal-Mogul Corporation show the effects of gas media density and supply voltage effects on the RF corona formation of the ACIS[47]. It indicates that the increase in gas media density significantly suppresses the corona discharge. It also suggests that the in-cylinder thermal and chemical processes can cause electronics control challenges. This is mainly attributed to the dramatic variations of the in-cylinder gas media conditions.

1.3.5 Plasma-assisted Combustion and Applications

The technique of RF corona ignition has raised much attention and has moved to the forefront of ignition research in the past few years. Plasma-assisted combustion is considered to be a promising technology to improve engine performance, stabilize lean burn flame, reduce exhaust emissions, and enhance low-temperature fuel oxidation, etc[52]. Over the last decade, significant progress has been made towards the understanding of the fundamental chemistry and dynamic processes in plasma-assisted combustion[55-55]. The results of streamer high frequency (HF) discharge[56] and nanosecond pulsed discharge (NPD)[57] have shown that plasma can enhance ignition, improve flame stabilization, and fuel/air mixing via chemical, thermal, and plasma-induced aerodynamic effects.

Although the above studies have successfully demonstrated the effectiveness of plasma in different areas, it remains uncertain that what kind of plasma is the most efficient for combustion enhancement[58]. Moreover, detailed plasma-combustion chemistry has not been well understood. It is also difficult to ascertain whether the observed enhancement is caused by the thermal or kinetic effect, owing to the large variation of plasma characteristics.

1.4 Thesis Outline

Chapter 1 begins with the motivation of improving ignition performance in lean/diluted combustion. Based on the advantages and limitations of conventional spark ignition systems, the advanced ignition systems are introduced by surveying the state-of-the-art ignition technologies. The background research in corona ignition is presented, which consists of the physical principles and recent applications of corona discharge. Furthermore, the existing corona ignition systems are briefed. The main benefits and

challenges of corona ignition are dutifully presented in due diligence. Lastly, the potential applications of corona-assisted combustion are proposed for automotive engines.

In Chapter 2, an in-house designed and fabricated AC corona system is presented in detail, in conjunction with the data acquisition method. Along with the commanded timeline, typical voltage and current waveforms of corona discharge are discussed. The author further undertakes the combustion tests in a constant volume combustion chamber (CVCC), with optical access to observe corona discharge formation, and to measure the electrical signal magnitude.

In Chapter 3, the effects on corona plasma length are characterized. Different parameters contain discharge voltage, frequency, duration, and background conditions.

Combustion tests under both the quiescent and flow conditions are presented in Chapter 4. The progress of flame kernel formation and early flame development are compared, by using spark ignition and corona ignition. A preliminary investigation of AC corona-assisted combustion is produced, mainly from empirical studies. The flame propagation processes are obtained by high-speed imaging.

In Chapter 5, the author provides a summary of the research conducted, lists the main conclusions, and proposes future work.

CHAPTER 2 EXPERIMENTAL SETUPS

In Chapter 2, an in-house designed AC corona discharge system is introduced in detail, including its electrical circuit, empirical setup, and ignition control. A data acquisition method for measuring the corona ignition system is presented, from which the typical voltage and current waveforms are derived and discussed. The author performs combustion tests in a constant volume combustion chamber (CVCC), with optical access to observe corona discharge formation, in addition to measure the electrical signal magnitudes per pressure variation. The original corona ignition system used in this work was devised by post-doctoral researcher Shui Yu at the University of Windsor Clean Combustion Engine Laboratory[59].

2.1 High-frequency Ignition Driver

A corona ignition system consists of three parts: an ignition driver, a high voltage resonator, and a corona igniter. The high-frequency ignition driver circuit, of 400 kHz to 4 MHz capability, is shown in Figure 2-1. The power driver converts direct current (DC) voltage with a range of 20~300 V to an AC voltage in the primary coil with a range of 300~ 500 V. This induces a higher potential AC voltage in the secondary coil around 5 ~ 15 kV. The frequency of the primary waveform is controlled by the transistor-transistor logic (TTL) signals. Ideally, a resonance is produced in the secondary circuit, thereby attaining the required voltage amplification.

The corona ignition system is mostly configured as a series-resonant R-L-C circuit, i.e. a resistor-inductor-capacitor circuit. The selection of operating frequency has wide-ranging effects on the performance of the system.

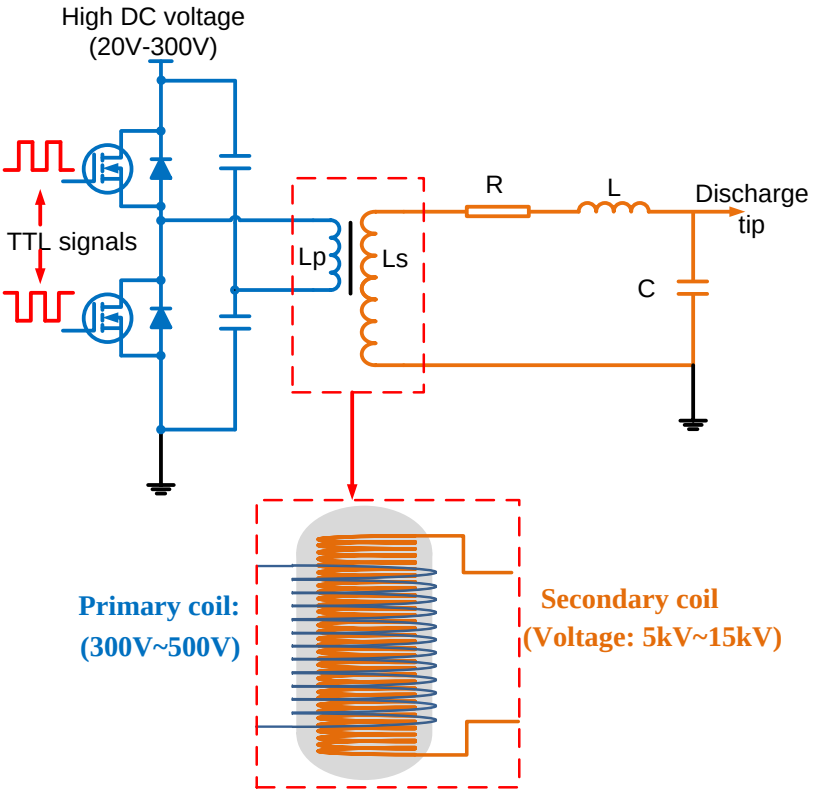

Figure 2- 1. A high-frequency ignition driver circuit of the corona ignition system.

It is known[19,60] that this series resonant circuit shown in Figure 2-1 will produce the maximum output voltage at a frequency given by:

$$f_r = \frac{1}{2\pi\sqrt{LC}} \tag{2.1}$$

where, f_r = Resonant frequency (Hz), L = Equivalent inductance (H), C = Equivalent capacitance (F).

At the resonant frequency, the capacitive and the inductive reactances counteract each other. The resultant impedance is a pure resistance[62]. The equations describing the relationship between the magnitude of impedance and circuit parameters, and the phase difference between the voltage and current signals are given below

$$|Z| = \sqrt{R^2 + \left(2\pi fL - \frac{1}{2\pi fC}\right)} \tag{2.2}$$

$$\emptyset = \tan^{-1}\left(\frac{2\pi fL - \frac{1}{2\pi fC}}{R}\right) \tag{2.3}$$

where $\emptyset$ is the phase difference between voltage and current signals, $|Z|$ represents the magnitude of the overall impedance of the R-L-C circuit. The phase difference between voltage and current signals is an important parameter for the energy calculation of corona discharge.

In the corona ignition system, it is often the case that the equivalent capacitance is difficult for a designer to apprehend. A corona igniter by body structure typically contributes to the majority of the capacitance in the circuit. In addition, unlike the conventional spark plugs, the combustion chamber surrounding a corona igniter is considered as the ground electrode. Thus, the capacitance in Figure 2-1 also includes the capacitance between the igniter tip to the combustion chamber. The corona ignitor will typically have an electrode with one or more relatively sharp tips, which is similar to the structure of signal releasing antennas. They are designed to produce locally high electric field strength from which corona forms.

2.2 Experimental Setup with a CVCC

A schematic of the empirical setup for the corona ignition system is shown in Figure 2-2.

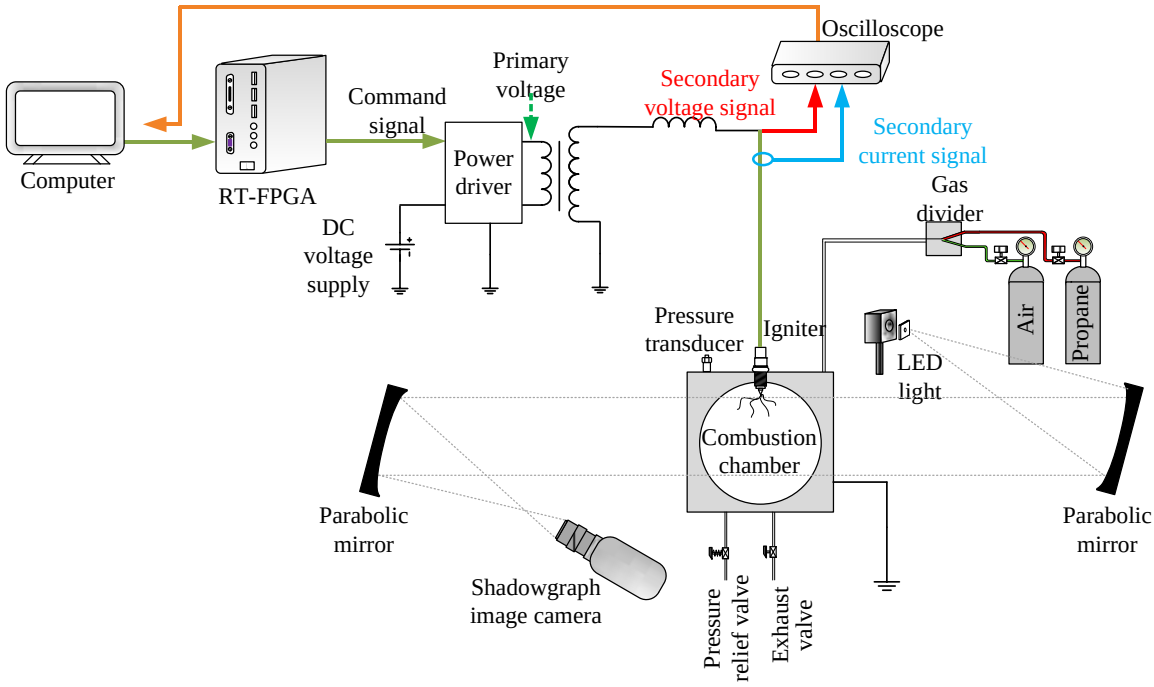

Figure 2- 2. Schematic of corona ignition system with shadowgraph imaging.

A set of combustion chambers of different sizes and functions are used. First, the corona discharge tests are conducted in an optical combustion chamber with a cylindrical inner volume of 25 mm in diameter and 25 mm in length. The chamber is operated under constant volume combustion conditions. Two recessed 1/4 inch ports are used for filling and exhausting the chamber. Two quartz windows with an 8 cm viewport in diameter provide an optical path through the chamber in the axial direction of the cylindrical volume. Second, tests with turbulence flow are conducted in an optical chamber with 0.2 liters in volume. The shadowgraph images are captured through two quartz windows with a 62 mm viewport in diameter.

The static pressure of the chamber is measured by a Swagelok PTI-S-NG5000-22AQ pressure sensor[19,61]. The dynamic pressure during a combustion process is measured by

a Kistler 6043A60 pressure sensor[19,61]. For the tests undertaken, the chamber is equipped with a rupture disk designed to stand 60 bar pressure.

The command TTL signals are controlled by an RT-FPGA, i.e. real-time field-programmable gate array. The sinusoidal AC voltage in the primary coil induces a higher potential AC voltage across the secondary coil. The required voltage amplification in the secondary circuit can be obtained by adjusting the frequency of the command signal.

2.3 Data Acquisition

2.3.1 Optical Data Acquisition

The flame kernel development is recorded by using a shadowgraph imaging system. The shadowgraph imaging setup consists of a Luminous Devices CBT-90 white LED light[19,61], a 0.4 mm pinhole aperture, two 6-inch f/8 parabolic mirrors, and a Vision Research Phantom V7.3 high-speed camera[19,61]. Parabolic mirrors are placed approximately nine feet apart on the opposing sides of an optical table. The LED light is placed at the focal point of one mirror, four feet apart, and approximately 10.5° off axis. The pinhole is placed immediately in front of the LED emitting surface. The camera is placed at the focal point of the second mirror, with an equal angle off the central axis.

The camera is typically run at a resolution of 256 × 256 to increase the frame rate to 36,697 fps. For tests using the CVCC, a Nikon 105 mm f/2.8 macro lens is used to match the image size to the active sensor area.

In addition to the shadowgraph imaging, direct imaging is performed with the camera placed in-line with the optical port and the lens focused on the igniter. Direct imaging is

used to capture the shape and color of the plasma generated by corona discharge. A consumer Canon 6D digital single-lens reflex camera is used to capture color and long-exposure images.

2.3.2 Numerical Data Acquisition

For the measurements of the high voltage at the secondary side, a Tektronix high-voltage probe with 1000:1 attenuation is used[19,60,61]. The discharge current is measured by an inductive Pearson 411 wide-band current monitor probe. The voltage and current signals are recorded by a PicoScope 4824 digital storage oscilloscope.

The measured points of the voltage and current signals are shown in Figure 2-2. The frequency of the command signal is set to 435 kHz. When the command signal is sent to the driver circuit, the amplitude of the secondary voltage and current will first increase before the values stabilize at certain levels. The electric oscillation within the secondary circuit of the corona ignition system sustains the corona discharge from the igniter tip.

An example of the command signal, measured secondary voltage signal, and measured secondary current signal is plotted in Figure 2-3. The waveforms of discharge voltage and current are sinusoidal waveforms with a phase difference. In an AC circuit, the instantaneous values of the voltage, current and therefore power are constantly changing. It is more convenient and easier on the maths to use the average or mean value of the power. Over a fixed number of cycles, the average value of the instantaneous power of corona discharge is simply given as:

$$P = V \times I \times \cos\theta \tag{2.4}$$

Where V and I are the Root-Mean-Square values of discharge voltage and current, and θ is the phase difference between the discharge voltage and the current. The units of power are in watts (W). The measured voltage and current signals are typically assumed to be traveling at the speed of light. In the experimental setup, the high-frequency ignition driver, the high-voltage probe, the current monitor and the coaxial cables for transmitting may cause the propagation delay for the signals displayed on the oscilloscope and subsequent measurement. The phase difference between the discharge voltage and current might change. Consequently, the calculation of the instantaneous power and discharge energy may be affected[60].

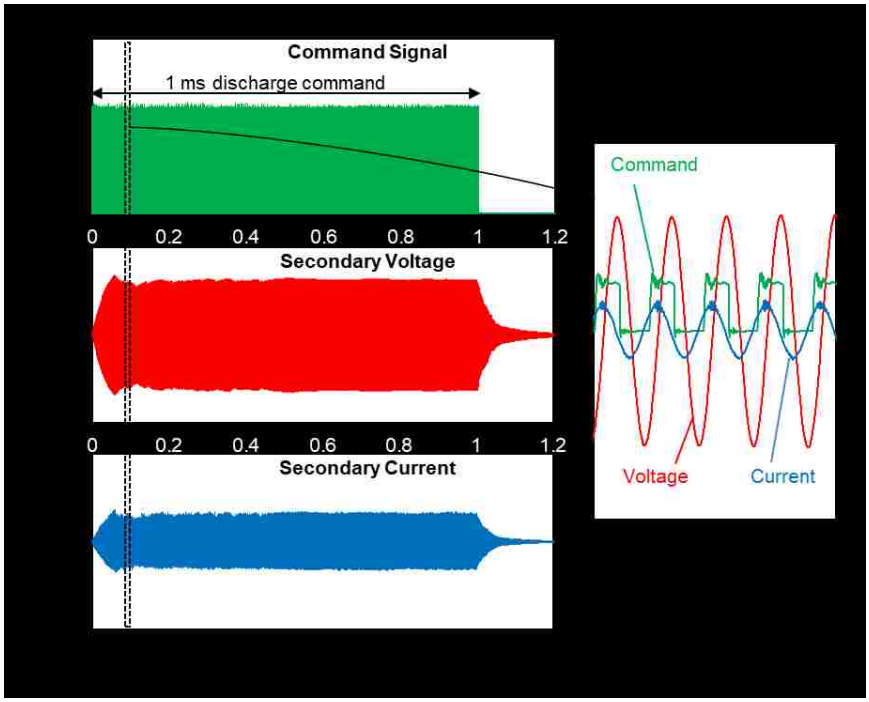

Figure 2- 3. The command signal, measured secondary voltage signal, and measured current signal during corona discharge.

CHAPTER 3 CHARACTERIZATION OF CORONA PLASMA LENGTH

In recent years, extensive research on RF corona ignition has revealed promising results in expanding the ignitability of lean/ diluted mixtures, producing potential gains in fuel efficiency. However, substantial physical challenges remain on the effective formation of corona[63]. In this chapter, the deployable length of corona streamers under the influence of various mixture conditions are characterized. The investigated parameters include the electric discharge voltage, frequency, duration, and the background pressure and composition.

3.1 Effect of Discharge Voltage

The electric voltage waveforms of corona discharge, under atmospheric conditions, are shown in Figure 3-1, in which comparisons are also made with the waveforms of spark discharge.

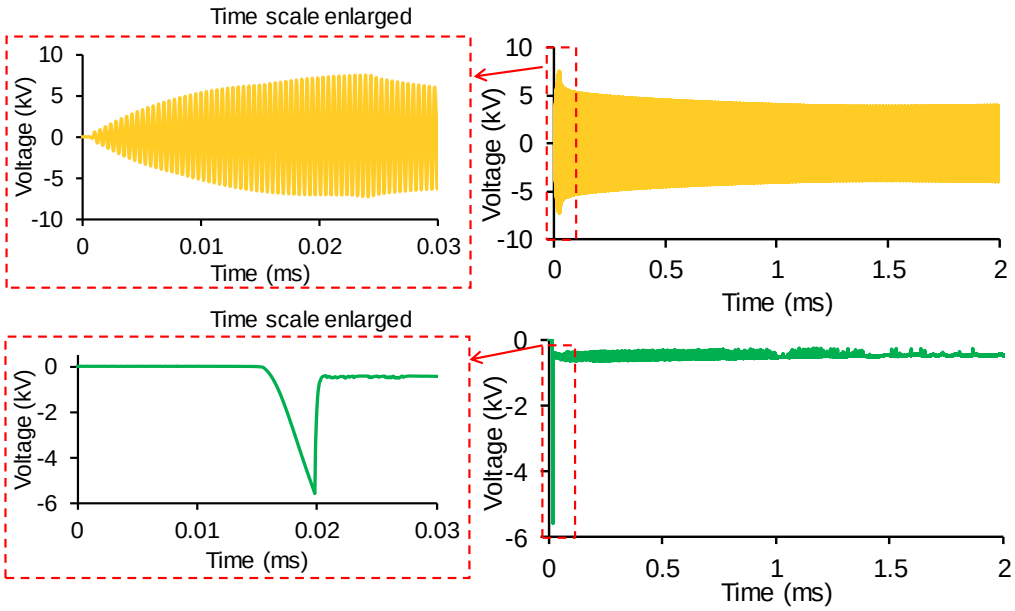

Figure 3- 1. The discharge voltage waveforms of corona vs. spark under atmospheric condition.

The discharge duration of the corona event is 2 ms. In comparison, the charging duration for the primary coil of the spark event is 2 ms, while the discharge duration of the secondary coil is a ballistic event of 1~2 ms depending on the coil and spark plug design, and background conditions.

The measurements are conducted for discharges in air at 2 bar absolute pressure. The breakout of corona discharge happens when the discharge voltage reaches a peak value after several cycles of resonance, which is shown in Figure 3-1. Using the present setup, the magnitude of the discharge voltage can be lifted by increasing the primary voltage. In this test, the breakout discharge voltage of corona is initially set at 8 kV. After the breakout, the waveform magnitude declines slightly and stabilizes until commanded off. Under the current setup, the corona will not release when the peak discharge voltage is lower than 8 kV. The normal corona discharge takes place when the peak discharge voltage is in the range of 8 kV to 10 kV, exceeding which an arcing event will be generated.

For a conventional TCI system, the spark sets off at the breakdown voltage across the spark gap. The comparison between the breakout discharge voltages of corona and the conventional spark is shown in Figure 3-2.

The breakout discharge voltage of corona under an increasing pressure presents an upward requirement which is similar to the breakdown voltage threshold of a conventional spark. Under a specific low pressure, the breakdown voltage of a spark event for the TCI system is lower than the breakout voltage of corona discharge, as observed in this study. However, the rising rate of the corona breakout discharge voltage

is lower as the background pressure rises, which leads to a relatively low breakout voltage of corona discharge under high pressures.

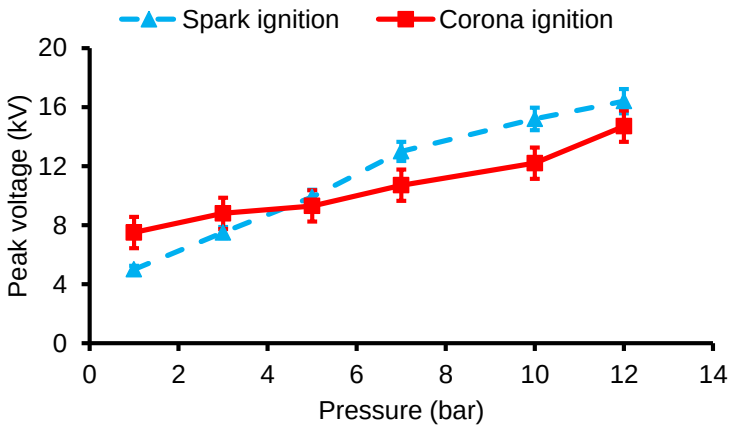

Figure 3- 2. The peak discharge voltages of corona vs. the breakdown voltages of conventional spark under different pressures.

When a command signal is sent to the power driver of the corona system, the secondary voltage and current will be devised to ascend oscillation until reaching certain values for apparent energy discharge. The continuous electric oscillation within the secondary circuit of the corona ignition system sustains the corona discharge from the igniter tip. In this work, the maximum length of the streamers released during corona discharge is ascribed as the length of the corona plasma. The direct images in Figure 3-3 show the streamer shapes of the corona plasma after the breakout under the moderately pressurized air using different discharge voltages. The corona discharge durations are 1 ms in all cases and the exposure time of the camera is 167 μs. As the discharge voltage rises from 4000 V to 9000 V, the strength of corona discharge tends to increase. The length of the corona plasma grows significantly.

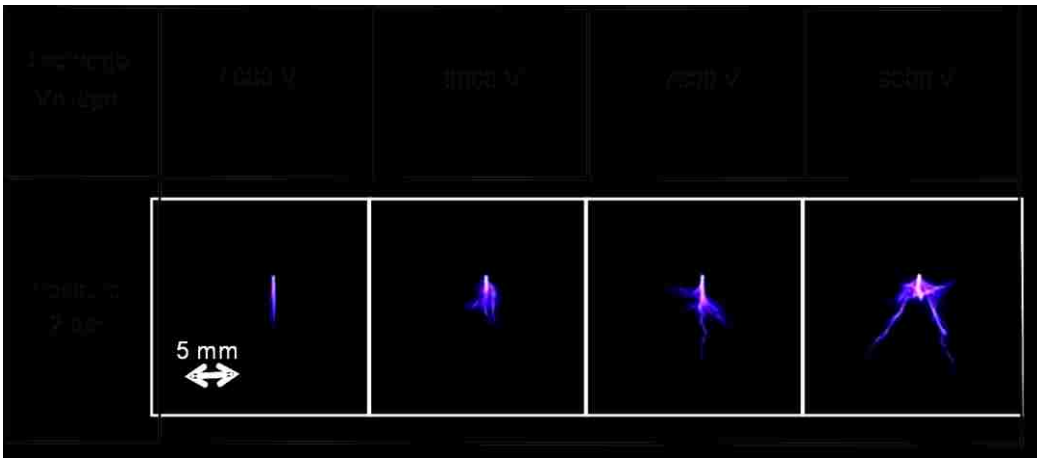

Figure 3- 3. The effect of discharge voltage on corona plasma length.

3.2 Effect of Discharge Duration

In addition to the increase of voltage to achieve stronger corona discharge, an increase in the duration of a discharge event is also a feasible way to improve the discharge performance via increasing the discharge energy. Figure 3-4 illustrates the corona discharge at 1 bar and 6 bar gauge pressure for discharge durations ranging from 0.1 ms to 4 ms.

At a discharge duration of 0.1 ms, the discharge is barely established and almost invisible. At a discharge duration of 0.25 ms, the substantial discharge penetration, under such pressure and voltage, is reached. Further duration increases result in a greater number of subsequent streamers, whereas the increase in pressure results in the streamer spatial coverage. When the discharge duration is increased to 2 ms and 4 ms, at a background of 1 bar gauge pressure, the corona discharge can be seen leading on the front surface of the ceramic support. This surface leaking discharge is suppressed at the higher pressure condition, however.

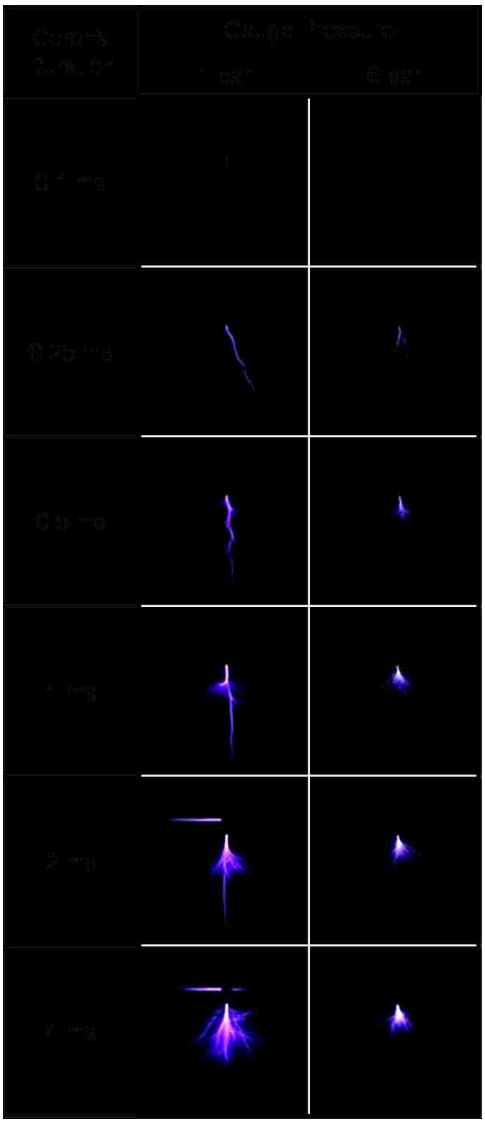

Figure 3- 4. Pressure and duration effect on corona plasma length.

3.3 Effect of Discharge Frequency

In this section, the primary voltage and discharge duration are kept constant. Under the testing conditions, the corona plasma length is also related to the frequency of the command signal within the selected frequency range (1.11~1.18MHz). The results are shown in Figure 3-5.

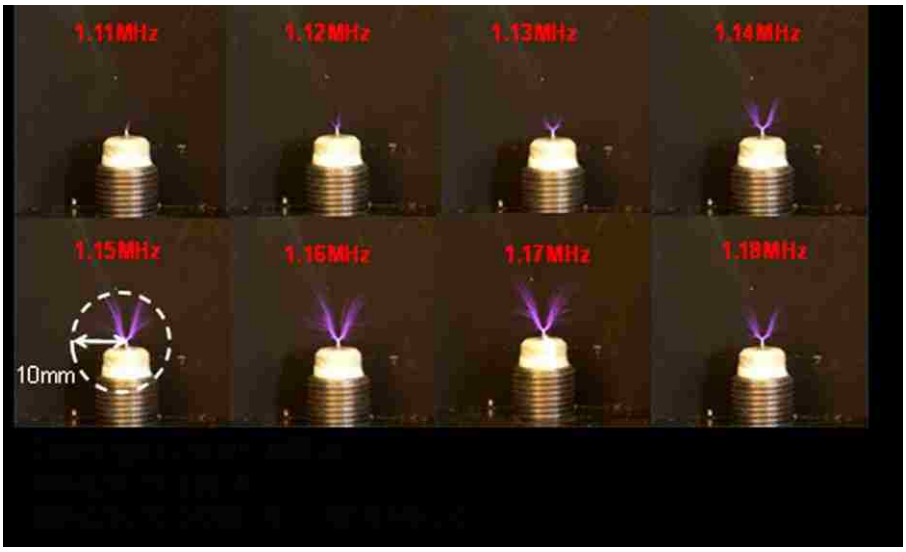

Figure 3- 5. The corona plasma length within the selected frequency range of the command signals.

In Figure 3-5, the length of corona plasma is ascribed as the radius of a circle in the 2-dimensional image, whose center is the igniter tip. The circle encloses all visible discharge streamers. The lengths of the corona plasma are plotted against frequency in Figure 3-6.

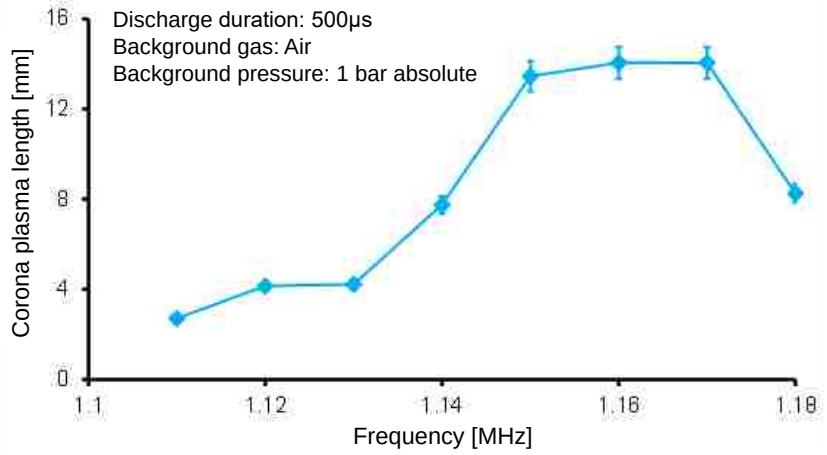

Figure 3- 6. The maximum length of the discharged streamers within the selected operating range of frequency.

As shown in Figure 3-5 and Figure 3-6, the length of corona plasma increases with the frequency, until the resonance frequency under this testing condition of 1.17MHz is reached. Thereafter, the streamers will shorten as the frequency further rises.

3.4 Effect of Background Media and Pressure

The length of corona plasma is strongly influenced by the background pressure. At a constant primary voltage, the streamer penetration is shorter under elevated pressures. Under higher pressures, the electrons and ions may lose energy by more frequent collisions, while the kinetic energy loss may hinder further ionization[64]. This can be partially overcome by increasing the electrical field strength through higher voltage under a fixed oscillation frequency.

The background gas type and pressure value often lead to different ionization coefficients, attachment coefficients, and the mobility status of the space charges. Thus, it is important to find out the influence of different background gases and pressures on the corona discharge. The direct images of corona discharge under various background conditions are shown in Figure 3-7, using helium, argon, and nitrogen gases. The input energy is kept the same by adjusting the primary voltage and discharge duration of the ignition system. In order to capture the whole discharge formation, the exposure time of the direct image camera and the corona discharge duration are set to 2 seconds and 50 ms, respectively, using a wide window to record a narrow event.

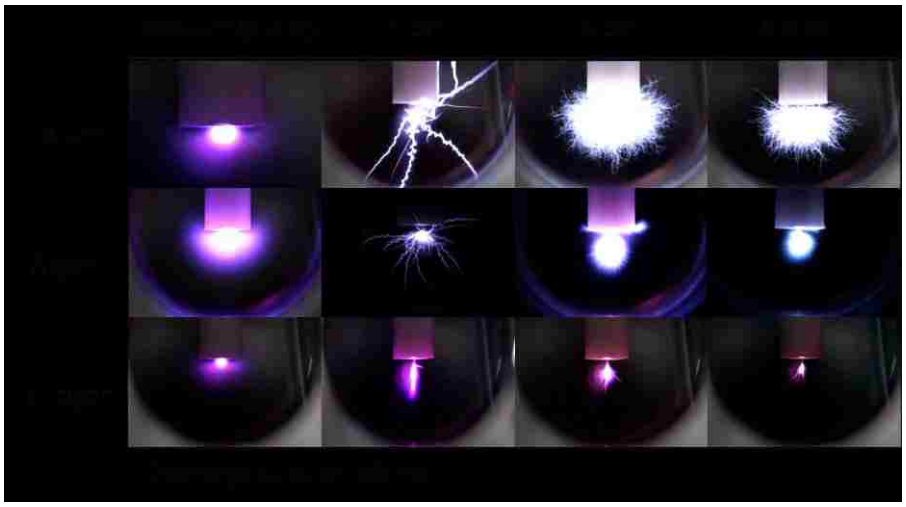

Figure 3- 7. Direct images of corona discharge using different background gases and under different pressures.

According to the direct images in Figure 3-7, the corona discharge under vacuum conditions tends to generate relative homogeneous plasma. The length of corona plasma can be affected by the gas components. When the pressure rises above atmospheric pressure, distinct corona streamers start to form. Plasma colors appear differently under different gases.

The corona discharge releases from the high voltage electrode, while the ground electrode is formed on the surrounding chamber surfaces. Thus, a fundamental advantage of the corona discharge is capable of providing long streamers that carry intensive energy. Besides the color and shape differences of corona plasma under different gases, the length of corona plasma, however, is observed to decrease as the pressure increases. Fundamentally, pressure rise means an increase in gas density. These direct images indicate that it is more difficult for corona to discharge stably under high pressures. Further investigations and discussions are required to explain the phenomenon quantitively.

In the circuit of Figure 2-1, the current-voltage relationship with the equivalent capacitance is

$$\frac{dV_c}{dt} = \frac{I_s}{C} \tag{3.1}$$

where V_c and I_s are the discharge voltage and current of the corona, respectively. As mentioned in Chapter 2, the equivalent capacitance includes the surrounding configuration of the corona igniter. Such equivalent capacitance is mainly affected by the gas composition and pressure in the combustion chamber. The duration of corona discharge is 40 μs. With the least square fitting method[65], the equivalent capacitance during corona discharge under different pressures is calculated and plotted in Figure 3-8.

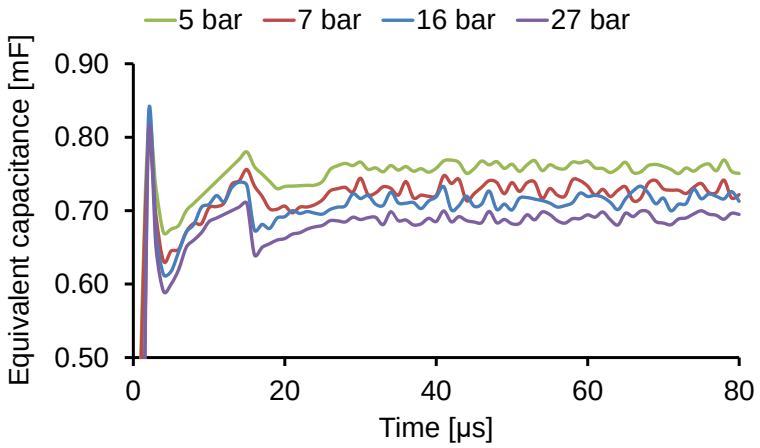

Figure 3- 8. The equivalent capacitance with corona discharge under different pressures.

As shown in Figure 3-8, under these testing conditions, the equivalent capacitances tend to be stable from 20 μs. After the corona discharge event with 40 μs duration, the lower background pressure 5 bar tends to form a larger equivalent capacitance. As it is shown in the above experimental results in this section, it is easier for corona to discharge with longer plasma lengths under low pressure. It might be easier for corona discharge with larger equivalent capacitance in the corona ignition system.

CHAPTER 4 IGNITION CAPABILITY OF CORONA DISCHARGE

The empirical research of the corona ignition of combustible mixtures is presented in Chapter 4. The results are divided into two parts, i.e. under quiescent and forced flow conditions in the constant volume combustion chamber. The flame kernel developments obtained from either spark or corona ignition are processed, and compared with each other. The effect of corona discharge on the flame kernel propagation is tested preliminarily and analyzed quantitatively. The flame propagation processes are recorded by the high-speed imaging, from which the flame areas are estimated using MATLAB software.

4.1 Effect of Discharge Voltage

In this section, the effect of primary voltage as a corona control parameter on the ignition event is examined. The experiments indicate that the corona discharge voltage has an impact on corona plasma length and streamer branching. The increasing strength of corona discharge may also influence the flame propagation. The corona discharge and subsequent flame propagation with the discharge duration of 80 μs and discharge voltage in the range of 4000 to 9000 V are shown in Figure 4-1. As shown in Figure 4-1, the flame expands faster with higher discharge voltage.

Under this testing condition, with the lowest discharge voltage of 4000 V, the corona discharge tends to generate three visible corona streamers in the image recorded. However, only one site of ignition occurs near the electrode tip. The sustainable flame kernel is formed near the electrode tip because of the high plasma intensity near the tip. The initial density gradients created in the other branches dissipate and fail to generate sites of flame kernels, after approximately 1 ms.

It is noted that when the discharge voltage is increased to 9000 V, even arcing is observed accessing from the igniter tip to the internal surface of the combustion chamber. Ignition occurs instantaneously along with the arcing streamer. Therefore, the discharge voltage adjusted by the primary voltage can be used as a control parameter to improve the flame propagation. In each test, the corona is released for 80 μs at 435 kHz under an absolute pressure of 2 bar.

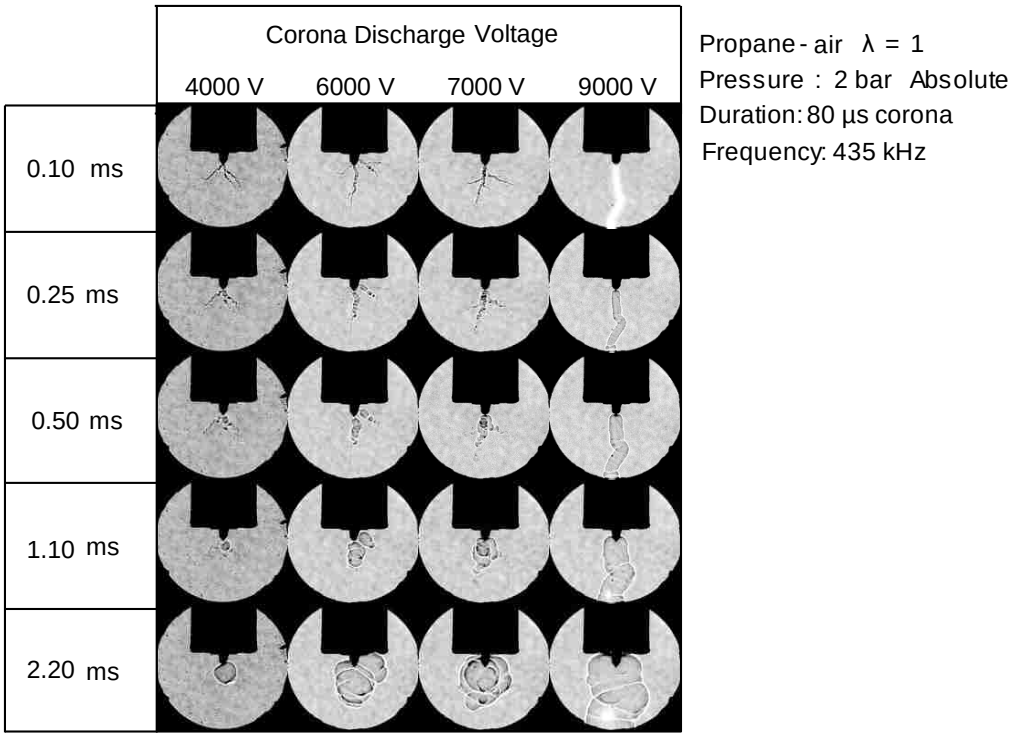

Figure 4- 1. Shadowgraph images of corona ignition in the propane-air mixture.

To quantify the flame propagation, the areas of the flame front from the 2D images are calculated and plotted in Figure 4-2. When the discharge voltage is 9000 V, the largest initial flame kernel and the fastest flame propagation are observed.

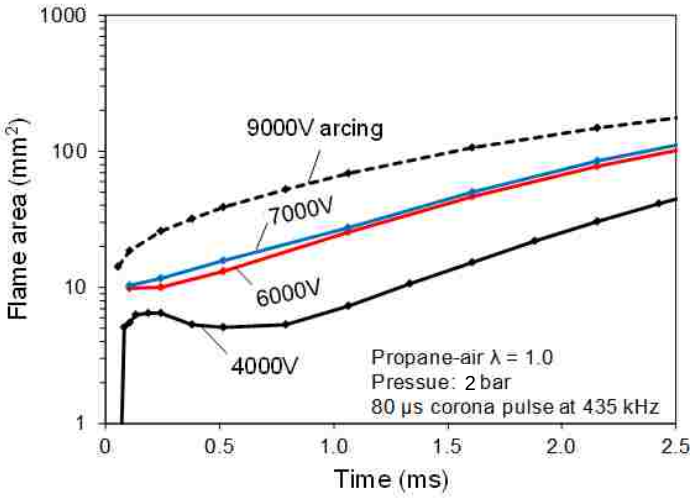

Figure 4- 2. Areas of the flame fronts under different discharge voltage levels.

The arcing event improves the flame formation of the air-fuel mixture in the demonstrated experiments. However, the high current surge during arcing may generate a considerable amount of heat which accelerates the wearing of the igniter tip.

4.2 Ignition Capability of Corona Discharge under Quiescent Conditions

Figure 4-3 compares the images of the ignition processes generated by a conventional spark with an RF corona discharge. Owing to the low energy level of the conventional spark discharge of 40 mJ in 1 ms, the initial flame kernel is smaller. In addition, the ground electrode seems to hinder the flame kernel development under the testing conditions. The flame kernel is still contained in the gap peripheral after 500 μs and exceeds the ground electrode after 1000 μs.

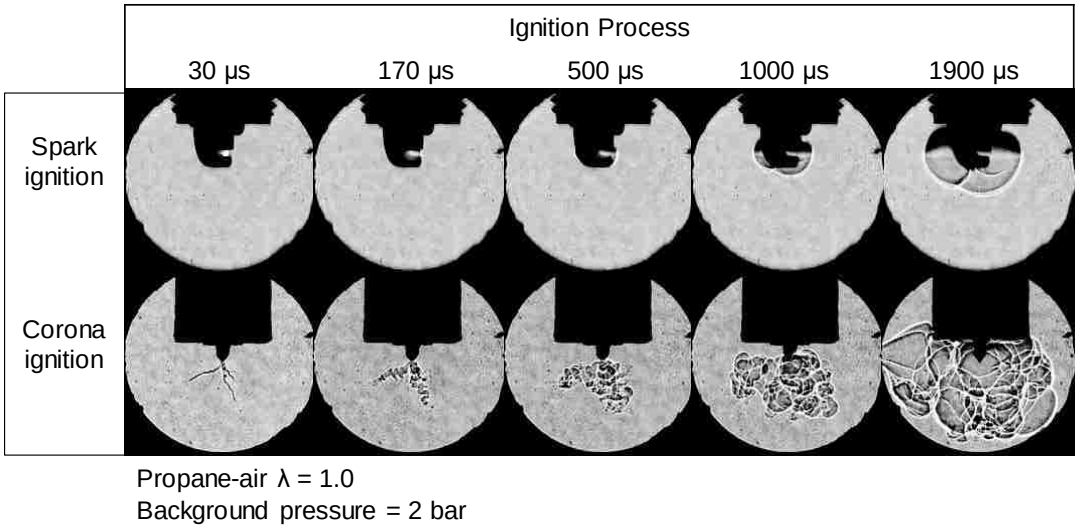

Figure 4- 3. Shadowgraph images of spark and corona ignition under quiescent condition.

In comparison, the effectiveness of the RF corona ignition system designed at the author's laboratory allows fast flame kernel formation and flame development. In stark contrast to the spark discharge, the corona discharge often produces multiple streamers. The flame kernel development is no longer hindered by an otherwise adjacent ground electrode. As a result, the flame early flame development of combustion can be significantly promoted, e.g. with the continuous supply of corona.

4.3 Ignition Capability of Corona Discharge under Forced Flow Conditions

The speed of flame propagation is reduced under lean/diluted conditions. In order to promote complete combustion, the enhancement of in-cylinder flow is an effective way to speed up the flame propagation. However, it is observed that the flow may bring more challenges to the spark ignition process[67]. Thereby, because the ignition volume of corona discharge is sufficiently large, the initial flame kernel can be sufficiently strong to form stable ignition processes. The high-speed shadowgraph images of spark ignition and corona ignition under forced flow conditions are shown in Figure 4-4. The charging

duration of the spark event is 4 ms and the discharge duration of the corona is 1 ms. The results show that, compared with the small ignition volume of conventional spark ignition, at least four streamers are formed of the corona discharge at an early stage, e.g. at 100 μs. As a result, the initial flame kernel and subsequent flame propagation are improved. Furthermore, under forced flow conditions, provided that the flame kernel formation sustains, the enhanced motion of the combustible mixture may speed up the flame propagation for both ignition cases.

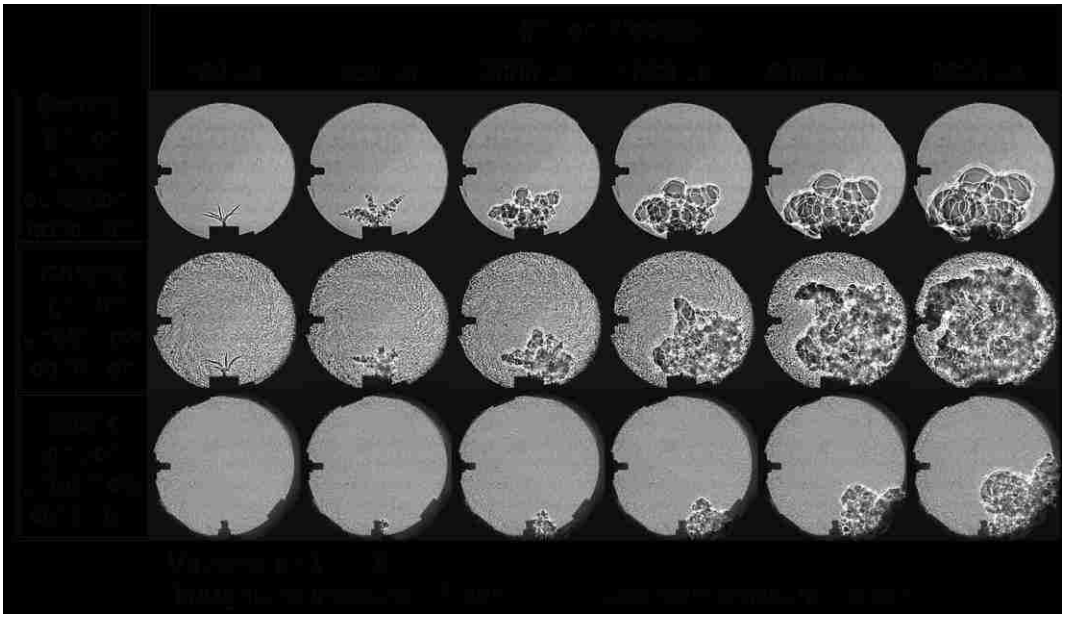

Figure 4- 4. Shadowgraph images of the spark and corona ignition cases under quiescent and forced flow conditions.

4.4 Flame Propagation Enhancement by Corona Discharge

In this section, the potential application of corona discharge on flame propagation enhancement is studied. The initial combustion flame is generated by the corona ignition with a discharge duration of 1 ms. At 3 ms, after the initial discharge onset, another

command of 1 ms pulse is added to the corona ignition system. As a result, the post corona discharge is released in presence of the formerly formed flame. In order to further characterize the effects of post corona discharge on flame propagation, a pulse train of four corona discharge events are applied to the initial combustion flame. The discharge currents under different conditions are shown in Figure 4-5. The baseline test is shown at the top of Figure 4-5, while discharge currents of one post and four post pulses assisted ignition events are plotted follow on.

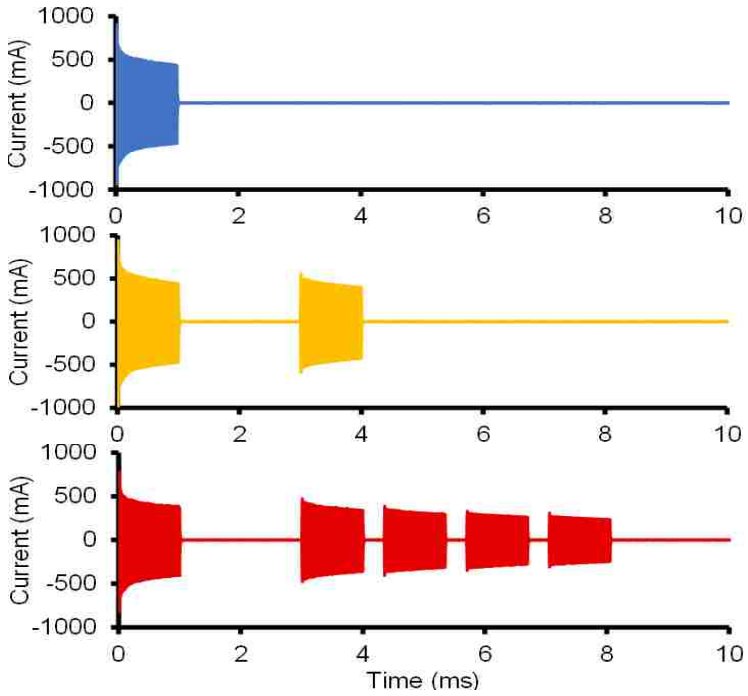

Figure 4- 5. Discharge currents of 1 ms corona ignition, one post and four post pulses corona-assisted ignition.

The scope of the corona discharge and flame development are demonstrated with the shadowgraph images in Figure 4-6. When a subsequent post pulse of corona discharge is applied, it is obvious that the existing flame is accelerated saliently. Moreover, the flame

surface pattern becomes progressively corrugated, which effectively increases the flame propagation.

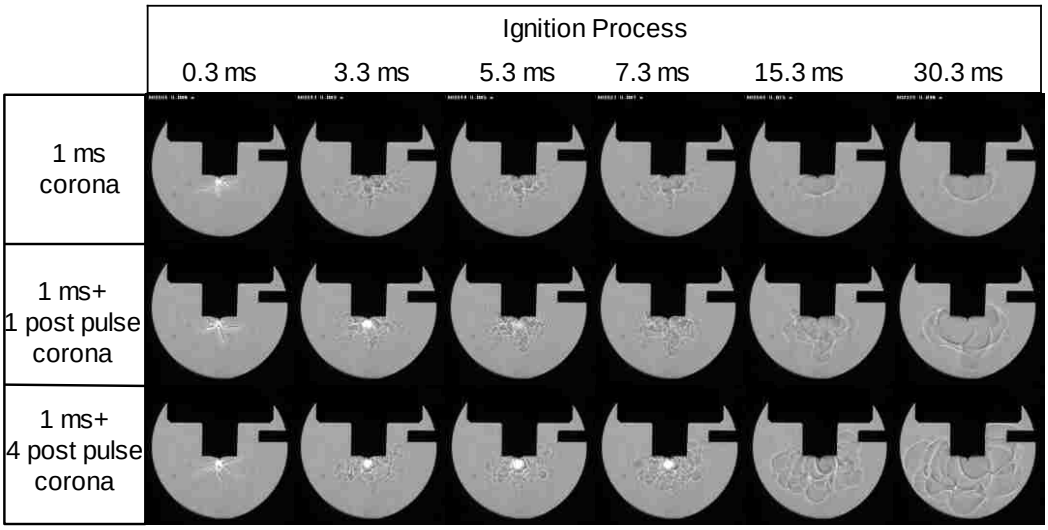

Figure 4- 6. Shadowgraph images of corona ignition and corona assisted flame propagation.

The quantitative values of the flame area in the shadowgraph images are shown in Figure 4-7, based on the results of the baseline corona ignition test and post corona assisted combustion tests. The increasing flame areas of the corona-assisted tests suggest the enhancement of combustion by the post corona pulses. On account of the ionized characteristics of the combustion flame, the AC electric field likely distorts the otherwise smooth flame front. Thus, stronger ion activation is generated, which enhances the speed of flame propagation. As it is discussed previously, besides the chemical influence, the thermal effect of the corona discharge may also speed up the flame kernel growth. Further fundamental research on the mechanism of corona-assisted combustion is necessary.

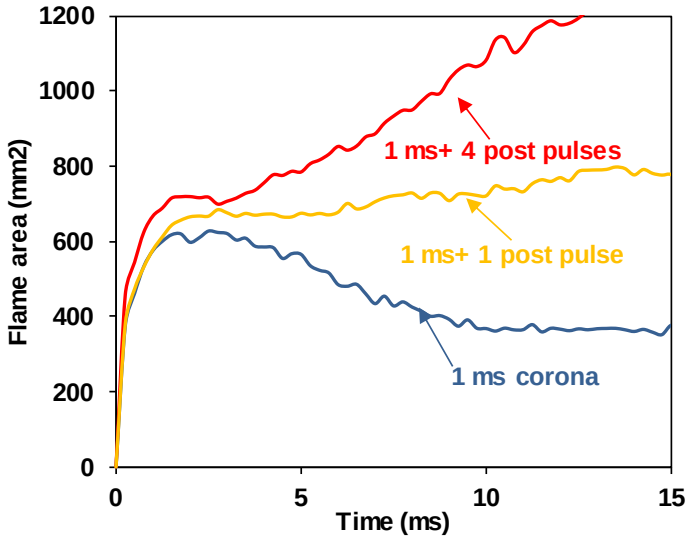

Figure 4- 7. Flame areas of corona ignition and corona assisted flame propagation.

CHAPTER 5 CONCLUSIONS AND FUTURE WORK

This chapter provides a summary of the main research results and the conclusions from the work performed. Recommendations for future research are also provided.

5.1 Conclusions

The corona discharge is considered to be one of the promising ignition methods to improve the performance of the lean/diluted combustion processes[4]. The setup of an in-house designed RF corona ignition system has been discussed and its parameter sensitivities have been demonstrated. By controlling stable corona discharge, the corona plasma length is characterized, including the effects of discharge voltage, discharge duration, discharge frequency, and background conditions on corona discharge. The ignition study has been conducted further to combustible mixtures. The ignition capabilities of corona discharge under both quiescent and forced flow conditions are demonstrated. The results are summarized below.

- The corona discharge provides larger ignition volume and its growth is impeded less due to the absence of a ground electrode. In a specific range, e.g. 8 kV~ 10 kV, the discharge voltage will generate normal corona discharge. However, the undervalued discharge voltage may not be sufficient to generate visible corona streamers and excessive discharge voltage may cause arcing.
- Within the normal RF power oscillation range, the increases of discharge voltage and duration will both result in a greater number of subsequent streamers and longer corona plasma length. At a constant discharge voltage and duration, the streamer penetration is shorter under elevated background pressures. The corona discharge will release longer streamers under the hardware resonance frequency.

- In this ignition research, the control and development of the flame kernel initiation are accomplished through the gating of corona discharge. The Increase of the corona discharge voltage generates the flame with the larger surface area. Provided that the flame kernel formation sustains, an enhanced motion of the combustible mixture may speed up the flame propagation.

5.2 Future Work

Based on the research in the past decades, RF corona discharge, e.g. electrostatic separation, used in the surface treatment industries [33,34], is considered as cold plasma. However, the temperature levels of corona discharge for ignition applications have been investigated insufficiently. In future work, the spectral analyses can be made to help quantify the characteristics of corona discharge plasma. The plasma temperature can be calculated with the Specair software[68]. The parameters that may affect the plasma temperature, such as discharge voltage, discharge duration, and background pressure et cetera, are recommended to be evaluated. More detailed tests and theoretical analyses are necessary for future research.

The closed-loop feedback control over combustion in actual internal combustion engines is very important, which can be made possible with the use of robust combustion sensing and diagnosing methods. The ion current measurement with a spark plug is one of the diagnosing methods. However, conventional spark plug based techniques have certain limitations. The spark plug gap, for instance, is optimized for spark discharge, rather than ion current measurement. Moreover, the measurement is limited to a single spatial location unless multiple sensors are installed. The flame propagation is slow and the density of detectable ions is low under lean or diluted conditions. The ion current

measurement with a spark plug may not be able to diagnose the ion signals under lean or diluted conditions. Additionally, the ion current signal is often blocked out by the spark current during the spark event.

As it is presented previously, without the presence of a spark plug gap, corona discharge is very sensitive to the surrounding environment. Different background gases and pressures in the combustion chamber may cause variations in the corona discharge. The gas density and temperature may lead to different ionizing capabilities of gas molecules. The preliminary investigations can be extended by the author, using corona discharge to perform the flame diagnoses in future research.

REFERENCES/BIBLIOGRAPHY

1. Z. Yang and A. Bandivadekar, “2017 Global Update: Light-Duty VehicleGreenhouse Gas and Fuel Economy Standards,” The International Council on Clean Transportation, 2017.
2. G. Kalghatgi, P. Risberg, and H. Ångström, “Partially Pre-Mixed Auto-Ignition of Gasoline to Attain Low Smoke and Low NOx at High Load in a Compression Ignition Engine and Comparison with a Diesel Fuel,” SAE Paper 2007-01-0006, 2007.
3. S. Kimura, O. Aoki, Y. Kitahara, and E. Aiyoshizawa, “Ultra-Clean Combustion Technology Combining a Low-Temperature and Premixed Combustion Concept for Meeting Future Emission Standards,” SAE Technical Paper Series, 2010.
4. M. Zheng and S. Yu, “Advanced Ignition Systems for Future Clean Combustion Engines: Review,” Journal of Automotive Saftey and Energy, 2015.
5. J. M. Beér, “Combustion technology developments in power generation in response to environmental challenges,” Progress in Energy and Combustion Science, 2000.
6. R. Herweg and R. R. Maly, “A Fundamental Model for Flame Kernel Formation in S. I. Engines,” SAE Technical Paper Series, 2010.
7. S. Imtenan, M. Varman and H. Masjuki, “Impact of low-temperature combustion attaining strategies on diesel engine emissions for diesel and biodiesels: a review,” Energy Convers Manage, 80: 329-356, 2014.
8. K. Kuo, “Principles of Combustion, 2nd ed,” Hoboken, NJ: Wiley, 2005.
9. J. Hilliard and G. S. Springer, “Fuel Economy in Road Vehicles Powered by Spark Ignition Engines,” New York: Plenum, 1984.
10. J. B. Heywood, “Internal combustion engines fundamentals,” McGraw-Hill Singapore, 1988.

11. R. R. Maly and R. Herweg, “Spark Ignition and Combustion in Four-Stroke Gasoline Engines,” Flow and Combustion in Reciprocating Engines, 1–66, 2008,

12. C. Hampe, H. Kubach and U. Spicher, “Investigations of ignition processes using high frequency ignition,” SAE Technical Paper, 2013-01-1633, 2013.

13. C. Hampe, M. Bertsch, K. Beck, U. Spicher, S. Bohne, G. Rixecker, “Influence of high-frequency ignition on combustion and emission behavior of small two-stroke spark ignition engines,” SAE Technical Paper, 2013-32-9144, 2013.

14. F. Wang, J. Liu, J. Sinibaldi, C. Brophy, A. Kuthi, C. Jiang, P. Ronney and A. Martin, “Transient plasma ignition of quiescent and flowing air/fuel mixtures,” IEEE Trans. Plasma Sci., vol. 33, no. 2 II, pp. 844–849, 2005.

15. X. Yu, Z. Yang, S. Yu, M. Ives, and M. Zheng, “Discharge Characteristics of Current Boosted Spark Events Under Flow Conditions,” Proceedings of the ASME 2017 Internal Combustion Engine Division Fall Technical Conference, 2017.

16. X. Yu, Z. Yang, S. Yu, X. Huo, D. Ting, M. Zheng, and L. Li, “Boosted Current Spark Strategy for Lean Burn Spark Ignition Engines,” SAE Technical Paper 2018-01-1133, 2018,

17. F. Marko, G. König, T. Schöffler, S. Bohne, and F. Dinkelacker, “Comparative Optical and Thermodynamic Investigations of High-Frequency Corona- and Spark-Ignition on a CV Natural Gas Research Engine Operated with Charge Dilution by Exhaust Gas Recirculation,” Ignition Systems for Gasoline Engines, pp. 293–314, 2016.

18. C. D. Cathey, T. Tang, T. Shiraishi, U. Urushihara, A. Kuthi, and M. A. Gundersen, “Nanosecond plasma ignition for improved performance of an internal combustion engine,” IEEE Trans. Plasma Sci., vol. 35, no. 6 PART 1, pp. 1664–1668, 2007.

19. S. Yu et al., “Multi-coil high-frequency spark ignition to extend diluted combustion limits,” Lecture Notes in Electrical Engineering, 2013.

20. M. Suess, M. Guenthner, M. Schenk, and H. Rottengruber, “Investigation of the potential of corona ignition to control gasoline homogeneous charge compression ignition combustion,” Proc. IMechE Part D: J. Automobile Eng. 226, 275–286, 2011.

21. T. Shiraishi, “Possibility of the new ignition system using the low-temperature plasma having dual functions of strengthening ignition for SI combustion and promoting and controlling autoignition of HCCI combustion,” Proceedings of First International Conference: Advanced Ignition Systems for Gasoline Engines, Berlin, Germany, 12–13 November 2012.

22. M. Kratzsch and M. Gunther, (eds.). 1st International Conference on Ignition Systems for Gasoline Engines, Berlin, 2012.

23. M. Gunther and R. Troger, (eds.) 2nd International Conference on Ignition Systems for Gasoline Engines, Berlin, 2014.

24. M. Schenk, M. Fessler, T. Wolf, B. Klaus, and H. Fischer, “Comparison of the thermodynamic Potential of alternative Ignition systems for SI-engines” Proceedings of First International Conference: Advanced Ignition Systems for Gasoline Engines, Berlin, Germany, 12–13 November 2012.

25. M. Suess, M. Guenthner, M. Schenk, and H-S. Rottengruber, “Investigation of the Potential of Corona Ignition to Control Gasoline Homogeneous Charge Compression Ignition Combustion,” Proceedings of the Institution of Mechanical Engineers, Part D: Journal of Automobile Engineering, 226: 275-286, 2012.

26. T. Wolf, M. Schenk, M. Schröter, F. Zellinger, B. Klaus, D. Pfeiffer, and H. Fischer, “RF-corona-ignition vs. spark ignition: a comparison for varying thermodynamic conditions and combustion strategies of modern turbocharged gasoline engines,” 2nd Symposium on Advanced Ignition Systems for Gasoline Engines, Berlin, Germany 2014.

27. T. J. Bonazza, K. L. VanVoorhies, and J. E. Smith, “RF Plasma Ignition System Concept for Lean Burn Internal Combustion Engines,” SAE Technical Paper Series, 2010.

28. E. Sher, J. Ben-Ya'ish, A. Pokryvailo, and Y. Spector, "A Corona Spark Plug System for Spark-Ignition Engines," SAE Technical Paper Series, 2010.

29. J. R. Roth, "Industrial Plasma Engineering," CRC Press, 2004.

30. R. B. Comizzoli, "Uses of Corona Discharges in the Semiconductor Industry," J. Electrochem. Soc., 2006.

31. Z. Machala et al., "Emission spectroscopy of atmospheric pressure plasmas for bio-medical and environmental applications," J. Mol. Spectrosc., 2007.

32. K. Yan et al., "Corona induced non-thermal plasmas: fundamental study and industrial applications," J. Electrostat., 1998.

33. J. Li, Z. Xu, and Y. Zhou, "Application of corona discharge and electrostatic force to separate metals and nonmetals from crushed particles of waste printed circuit boards," J. Electrostat., 2007.

34. J. Ryu, T. Wakida, and T. Takagishi, "Effect of Corona Discharge on the Surface of Wool and Its Application to Printing," Text. Res. J., 1991.

35. Y. H. Lee et al., "Application of pulsed corona induced plasma chemical process to an industrial incinerator," Environ. Sci. Technol., 2003.

36. S. Masuda, M. Hirano, and K. Akutsu, "Enhancement of electron beam denitration process by means of electric field," Radiat Phys Chem, 17:223–228, 1981.

37. S. Masuda, H. Nakao, "Control of NOx by positive and negative pulsed corona discharges," IEEE Trans Ind Appl 26:374–383, 1990.

38. C. Hampe, M. Bertsch, K. W. Beck, et al., "Influence of high-frequency ignition on the combustion and emission behavior of small two-stroke spark ignition engines," SAE Tech Paper, 2013-32-9144, 2013.

39. G. Bachmaier, R. Baumgartner, D. Evers, R. Freitag, T. Hammer, and G. Lins, "Radio frequency ignition system for gasoline direct injection engines," Int. J. Plasma Environ. Sci. Technol., vol. 6, no. 2, pp. 140–148, 2012.

40. D. Bradley and S. H. Nasser, “Electrical coronas and burner flame stability,” Combust. Flame, vol. 55, no. 1, pp. 53–58, 1984.

41. J. Liu, F. Wang, L. Lee, P. Ronney, and M. Gundersen, “Effect of Fuel Type on Flame Ignition by Transient Plasma Discharges,” 2013.

42. J. Burrows, J. Lykowski, and K. Mixell, “Corona ignition system for highly efficient gasoline engines,” MTZ Worldw., 2014.

43. B. Steffen, R. Georg, B. Volker, and B. Michael, “High-Frequency Ignition System Based on Corona Discharge,” MTZ worldwide. 75, 10.1007/s38313-014-0007-1, 2014

44. A. Cimarello, C. Grimaldi, F. Mariani, M. Battistoni, et al., “Analysis of RF Corona Ignition in Lean Operating Conditions Using an Optical Access Engine,” SAE Technical Paper 2017-01-0673, 2017.

45. C. A. Idicheria and P. M. Najt, “Potential of Advanced Corona Ignition System (ACIS) for Future Engine Applications,” Ignition Systems for Gasoline Engines, 2016.

46. A. Mariani and F. Foucher, “Radio frequency spark plug: An ignition system for modern internal combustion engines,” Appl. Energy, vol. 122, pp. 151–161, 2014.

47. J. Burrows, K. Mixell, P. Reinicke, et al., “Corona Ignition – Assessment of physical effects by pressure chamber, rapid compression machine, and single cylinder engine testing,” 2nd Int Conf Ignition Syst for Gasoline Engines, November 24–25, 2014, Berlin, Germany.

48. H. Nouri, N. Zouzou, E. Moreau, L. Dascalescu, Y. Zebboudj, “Effect of relative humidity on current-voltage characteristics of an electrostatic precipitator,” Journal of Electrostatics, vol 70, no. 1, pp. 20-24, 2012.

49. M. Abdel-Salam and N. L. Allen, “Current-voltage characteristics of corona in rod-plane gaps as influenced by temperature,” IEE Proceedings - Science, Measurement and Technology, vol. 150, no. 3, pp. 135-139, 2 May 2003.

50. P. Krüger and B. Visser, “Advanced Plasma Ignition (API): A Simple Corona and Spark Ignition System,” in Ignition Systems for Gasoline Engines, pp. 260–264. 2016.

51. E. A. Yahaya, “Power loss due to Corona on High Voltage Transmission Lines,” IOSR J. Electr. Electron. Eng., vol. 8, no. 3, pp. 14–19, 2014.

52. Y. Ju and W. Sun, “Plasma-assisted combustion: Dynamics and chemistry” Progress in Energy and Combustion Science, vol. 48. pp. 21–83, 2015.

53. S. A. Bozhenkov, S. M. Starikovskaia, and A. Y. Starikovskii, “Nanosecond gas discharge ignition of H_2 - and CH_4 - containing mixtures,” Combust. Flame, 2003.

54. F. Zhang, Z. Ren, S. Zhong, M. Yao, and Z. Peng, “Role of low-temperature fuel chemistry on turbulent flame propagation,” Wuli Huaxue Xuebao/ Acta Phys. - Chim. Sin., 2019.

55. A. Czernichowski, “Gliding arc: Applications to engineering and environment control,” Pure Appl. Chem., vol. 66, no. 6, pp. 1301–1310, 1994.

56. A. Klimov, V. Bityurin, A. Kuznetsov, B. Tolkunov, N. Vystavkin, and M. Vasiliev, “External and Internal Plasma- Assisted Combustion,” 2013.

57. H. Do, S. K. Im, M. A. Cappelli, and M. G. Mungal, “Plasma-assisted flame ignition of supersonic flows over a flat wall,” Combust. Flame, vol. 157, no. 12, pp. 2298–2305, 2010.

58. Y. Ju, H. Guo, K. Maruta, and F. Liu, “On the extinction limit and flammability limit of non-adiabatic stretched methane-air premixed flames,” J. Fluid Mech., 1997.

59. M. Zheng, S. Yu, and M. Wang, US Patent 9,484,719 (Application 14/329,628). “Active Control Resonant Ignition System.” 128 Divisional patent filed Oct 5, 2016.

60. R. Akshay, “Modeling of Corona Ignition System,” Electronic Theses and Dissertations. 7391, 2018.

61. K. Xie, “Effective Ignition Control in Advanced Combustion Engines,” Electronic Theses and Dissertations. 7486, 2018.

62. J. Burrows and K. Mixell, “Analytical and Experimental Optimization of the Advanced Corona Ignition System,” in Ignition Systems for Gasoline Engines, 2016.

63. S. Yu, K. Xie, X. Yu, M. Wang, et al., “High Energy Ignition Strategies for Diluted Mixtures via a Three-Pole Igniter,” SAE Technical Paper, 2016-01-2175, 2016.

64. P. Slade, “Electrical Contacts: Principles and Applications, Second Edition,” CRC Press. ISBN 9781439881309, 2013.

65. L. Wang, Y. Jia, T. Chai, and W. Xie, “Dual-Rate Adaptive Control for Mixed Separation Thickening Process Using Compensation Signal Based Approach,” IEEE Trans. Ind. Electron., vol. 65, no. 4, pp. 3621–3632, 2018.

66. S. Yu, K. Xie, Q. Tan, M. Wang, and M. Zheng, “Ignition Improvement of Premixed Methane-Air Mixtures by Distributed Spark Discharge,” in SAE Technical Paper Series, 2015.

67. Z. Yang et al., “Impacts of Spark Discharge Current and Duration on Flame Development of Lean Mixtures Under Flow Conditions,” p. V001T03A032, 2019.

68. S. Huang, T. Li, Z. Zhang and P. Ma, “Rotational and vibrational temperatures in the spark plasma by various discharge energies and strategies” Applied Energy. 2019. 251-113358, 251. 10.1016/j.apenergy.2019.113358.

APPENDICES

Appendix A

A schematic diagram of the averaged electron temperature and electron number density is shown in Figure A-1 for different types of plasmas, corona, direct current (DC) discharge, microwave (MW) discharge; dielectric barrier discharge (DBD), radio-frequency discharge (RF), glow discharge, gliding arc, nanosecond pulsed discharge (NSD), arc, magneto-hydrodynamic discharge (MHD), and flame[52]. The electron temperature and number density of plasma are governed by the reduced electric field (E/N, the electric field strength divided by the molecular number density).

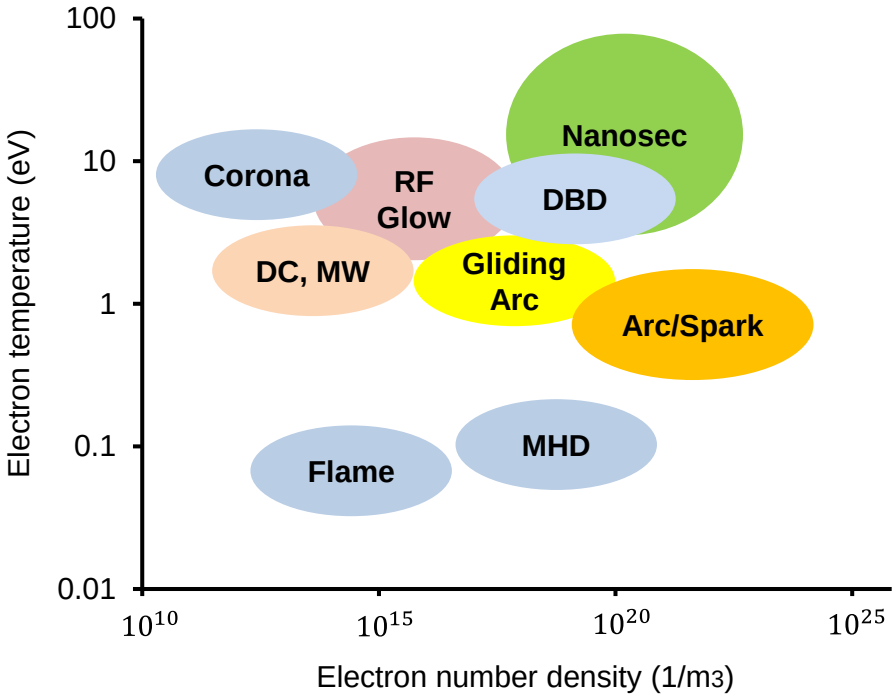

Figure A-1. Schematic of electron temperature and number density for different discharges.

Appendix B

Matlab code of phase difference calculation

```
clear
clc
Date='20190624-';
for j=4
   if j<10
      filename=['000',num2str(j)];
   else
      filename=['00',num2str(j)];
   end
Title=[Date,filename,'.csv']

time=csvread(Title,4,0,[4,0,10000,0])/1000;% ms
%%
chA=csvread(Title,4,1,[4,1,10000,1]);% trigger, V
chE=csvread(Title,4,2,[4,2,10000,2])*10;% current A
chG=csvread(Title,4,3,[4,3,10000,3]);%k voltage

Sampletime=0.0001;
Fs=1/Sampletime;%(time(2)-time(1));%sampling frequency
dchA=diff(chA);
rR=find(dchA>1);
rF=find(dchA<-1);

rS=rR(1);%locate active signal starting point
rE=length(time);%locate active signal ending point

ntime=time(rS:rE);
nA=chA(rS:rE);
nE=chE(rS:rE);
nG=chG(rS:rE);
[Aa,Bb] = butter(2,0.7);
fnA=filtfilt(Aa,Bb,nA);
fnE=filtfilt(Aa,Bb,nE);
fnG=filtfilt(Aa,Bb,nG);
mnA=mean(fnA);
fnA=fnA-mnA;

Peakc=find(fnE==max(fnE));
Peakt=ntime(Peakc)
plot(ntime,fnE,'r')
set(gca, 'FontName', 'Arial', 'FontSize', 14)
xlabel('Time(ms)')
```

```
ylabel('Current(A)')
xlim([0 0.02])

n=0;

for i=2:1:length(fnE)-1

 if fnE(i-1)*fnE(i+1)<0
     n=n+1;
   flag(n)=i;
 end

 if n>1

 if flag(n)-flag(n-1)==1
   n=n-1;
end
end
end
mtime(1)=0;
n=1;
for i=1:2:length(flag)
   if i+2>length(flag)
      break
   else
   [~,Aloc(n)]=min(fnA(flag(i):flag(i+2)));
   [~,Eloc(n)]=min(fnE(flag(i):flag(i+2)));
   [~,Gloc(n)]=min(fnG(flag(i):flag(i+2)));
   cycle(n)=flag(i+2)-flag(i);
   mtime(n+1)=mtime(n)+cycle(n)/1000;
   n=n+1;
   end
end

[Mm,Nn] = butter(2,0.2);

PhaseG_A=(Gloc-Aloc).*360./cycle;
fPhaseG_A=filtfilt(Mm,Nn,PhaseG_A);

PhaseG_E=((Gloc-Eloc).*360./cycle);
fPhaseG_E=filtfilt(Mm,Nn,PhaseG_E);

PhaseH_Eb=mean(fPhaseG_E);
PhaseH_Ea=mean(fPhaseG_E);
end
```

Matlab code of flame area calculation

```
clear
clc

mainfolder = pwd;% cd('processed')
mkdir('bksub')
initial='_000';
format='bmp';
tr_left=0;
tr_right=0;
tr_top=30;
tr_bottom=0;
background_img=imread('_000001.bmp');

area=zeros(10,1);
cell_count=zeros(10,1); %amount of cells that exhibit light
int_total=zeros(10,1);
int_avg=zeros(10,1);

Injfiles = dir(fullfile(mainfolder, '*.bmp'));
img_total=length(Injfiles)-2;
for j=1:img_total
   if j<10
      filename=[initial,'00',num2str(j),'.',format];
   end
   if j<100&j>=10
      filename=[initial,'0',num2str(j),'.',format];
   end
   if j<1000&j>=100
      filename=[initial,num2str(j),'.',format];
   end

   img_curr_full=imread(filename);
   img_curr_sub=(img_curr_full-background_img)*1;

   [x,y]=size(img_curr_sub);
   img_curr_sub=img_curr_sub(tr_top+1:x-tr_bottom,tr_left+1:y-tr_right);

   bb=img_curr_sub;
   for i=1:3
      se=strel('disk',4);
      hh=imdilate(bb,se);
      bb=hh;
   end
   see=strel('disk',4);
```

```
    hd=imclose(hh,see);
    hh=hd;

   hdd=imfill(hd,'holes');
    hd=hdd;

    pix_orig=hd;
    pix_orig(find(pix_orig<=15))=0;

    hd(find(hd>15))=255;
    hd(find(hd<=15))=0;
    hd = bwperim(hd,8);
    hdd=imfill(hd,'holes');
    area(j,1)=bwarea(hdd)*0.0259;
        cell_count(j,1)=sum(sum(pix_orig>0)); %amount of cells that exhibit light
        int_total(j,1)=sum(sum(pix_orig));
        int_avg(j,1)=int_total(j,1)/cell_count(j,1); %light intensity per cell with any bit of
    cd('bksub')
     imwrite(hdd,filename,format);
    xlswrite('area-8.xls', [area, int_total, cell_count]);
    cd(mainfolder)
end
t=[1:img_total]'*27.5/1000;
```

LIST OF PUBLICATIONS

Journal Publications

1. YUAN Zhe; WANG Yong-Zhen; SHI Huai-Tao; XIAO Jian-Yu; **WANG Lin-Yan**. The Maximum Connected Rectangle of Any Graph Based on Improved Genetic Algorithm. Control Engineering of China, 2016, 3: 400-404.

2. WU Cheng-Rui, JIA Yao, **WANG Lin-Yan**. A Hardware-in-the-Loop Simulation System in Mixed Separation Process. Chinese Journal of Engineering, 2017, 9: 1412-1420.

3. **WANG Lin-Yan**, JIA Yao, CHAI Tian-You. A Double-Rate Intelligent Switching Control for Mixed Separation Thickening Process. Acta Automatica Sinica, 2018, 2: 330-343.

4. **WANG Lin-Yan**, JIA Yao, CHAI Tian-You. Dual-Rate Adaptive Control for Mixed Separation Thickening Process Using Compensation Signal Approach, IEEE Transactions on Industrial Electronics, 2018, 65, 4.

Conference Papers

5. **WANG Lin-Yan**, JIA Yao, CHAI Tian-You. A Data Driven Double-Rate Switching Control for Mixed Separation Thickening Process. The 27th Chinese Process Control Conference (July 2016).

6. **WANG Lin-Yan**, JIA Yao, CHAI Tian-You. Dual Rate Adaptive Control for Mixed Separation Thickening Process Using Compensation Signal Approach, The 28th Chinese Process Control Conference (July 2017), the finalist for the Zhongjun Zhang Academician Excellent Paper Award.

7. D. Purohit, S. Dev, Q. Tan, N. Sandhu, **L. Wang**, G. Reader, M. Zheng. An Investigation on the Regeneration of Lean NOx Trap using Ethanol and n-Butanol, 2019 WCX SAE World Congress Experience.

8. **WANG Lin-Yan**, TAN Qing-Yuan, YU Shui, YU Xiao, CHEN Xiang, ZHENG Ming. A Framework for the Active Control of Corona Ignition Systems. 2019 JSAE/SAE Powertrains, Fuels, and Lubricants International Meeting.

VITA AUCTORIS

NAME:	Linyan Wang
PLACE OF BIRTH:	Shenyang, China
YEAR OF BIRTH:	1992
EDUCATION:	Northeastern University, B.Sc., Shenyang, China, 2015
	Northeastern University, M.Sc., Shenyang, China, 2018